Optimization of Mixed Helical-Labyrinth Seal Design to Improve the Efficiency of a Machine

---

A Thesis

Presented to

The faculty of the School of Engineering and Applied Science

University of Virginia

In partial fulfillment

Of the requirement for the degree

Master of Science

(Mechanical and Aerospace Engineering)

By:

Wisher Paudel

December

2018

ABSTRACT

Non-contacting annular seals are used in rotating machinery to reduce the flow of fluid across a pressure differential. Helical and labyrinth groove seals are two types of non-contacting annular seals frequently used between the impeller stages in a pump. Labyrinth seals have circumferential grooves cut into the surface of the rotor, the stator, or both. They function to reduce leakage by dissipating kinetic energy as fluid expands in the grooves and then is forced to contract in the jet stream region. Helical groove seals have continuously cut grooves in either or both of the rotor and stator surfaces. Like labyrinth seals, they reduce leakage through dissipation of kinetic energy but also have the added mechanism of functioning as a pump to push the fluid back towards the high pressure region as it tries to escape. Several works in literature have shown that labyrinth and helical groove seals with grooves on both the rotor and the stator surfaces have lower leakage than seals with grooves on just one surface.

The goal of this work is to analyze seals with helical grooves on one surface and labyrinth grooves on the other for both high pressure and low pressure applications. Designs for both helical stator, labyrinth rotor and helical rotor, labyrinth stator are simulated and the performance of each configuration is compared. The primary variables considered for the designs of the seals include the width, depth, and the number of grooves for labyrinth seals and the width, depth, and the angle of the grooves for helical seals. The set of simulation designs is chosen using a Kennard-stone algorithm to optimally space them within the design space. Then, for both configurations, multi-factor quadratic regression models are generated. Backward regression is used to reduce the models to only statistically significant design parameters. From there, the response surfaces are created to demonstrate the effects of each design parameter on

the performance of the seal. Finally, an optimal design is produced based on the regression models.

The designs are simulated to show the predictive power of the regression models. The simulations for this work are run in ANSYS CFX for each seal type and configuration and the solutions are compared against those from previous studies. The findings from this study were hypothesized to show substantial decrease in leakage for a mixed helical-labyrinth seals in comparison to the seal with either helical or labyrinth grooves on both surfaces. Thus, the effectiveness of mixed helical-labyrinth grooved seals is highlighted for both low and high pressure cases and their efficiency and reliability for numerous industrial applications.

ACKNOWLEDGEMENTS

I would like to acknowledge the financial support from the Rotating Machinery and Controls (ROMAC) industrial program. I would like to thank my advisor Dr. Houston Wood for accepting me into the graduate program and allowing me to perform this work for ROMAC. Additionally, I am really appreciative of Dr. Cori Watson for all of her help and guidance throughout this project. Thank you to Dr. Roger Fittro and Dr. Daniel Quinn for agreeing to be part of my defense committee. Finally, thanks to my Mom, Saraswati, Dad, Bishnu, brother, Bikal, and all of my friends for their continuing support during my graduate studies.

TABLE OF CONTENTS

TABLE OF FIGURES

TABLE OF TABLES

CHAPTER 1: INTRODUCTION

Leakage of a working fluid is one of the primary concerns that need to be addressed while designing pumps, compressors, or any turbomachinery. If not controlled, fluid leakage can introduce costly problems including corrosion and bearing fatigue, product loss, personnel safety, and pollution. In order to alleviate the aforementioned issues, seals are commonly applied to a machine to contain any liquid or gas within a vessel where there is a rotating shaft and a stationary housing. There exist a variety of seals in industry that can be used for specific applications. This thesis focuses on non-contacting mechanical annular seals that provide advanced sealing capabilities for rotating shafts.

Non-contacting annular seals are used in pumps and other turbomachinery to reduce the leakage of the working fluid across a pressure differential on each impeller stage. The leakage of a seal at a given pressure differential is directly correlated to the efficiency of the machine. Non-contacting seals are often selected for cases where contact between different machine parts could result in too much frictional force or when total prevention of leakage is not required. The latter is the case for liquid pumps, which is the application this thesis focuses on. The two main types of seals that form the core of this work are helical and labyrinth seals.

Both helical and labyrinth groove seals resist flow through dissipation of kinetic energy as fluid flowing axially down the seal expands in the grooves and then is forced to contract in the jet stream region between the grooves. This path is shown in Figure 1.

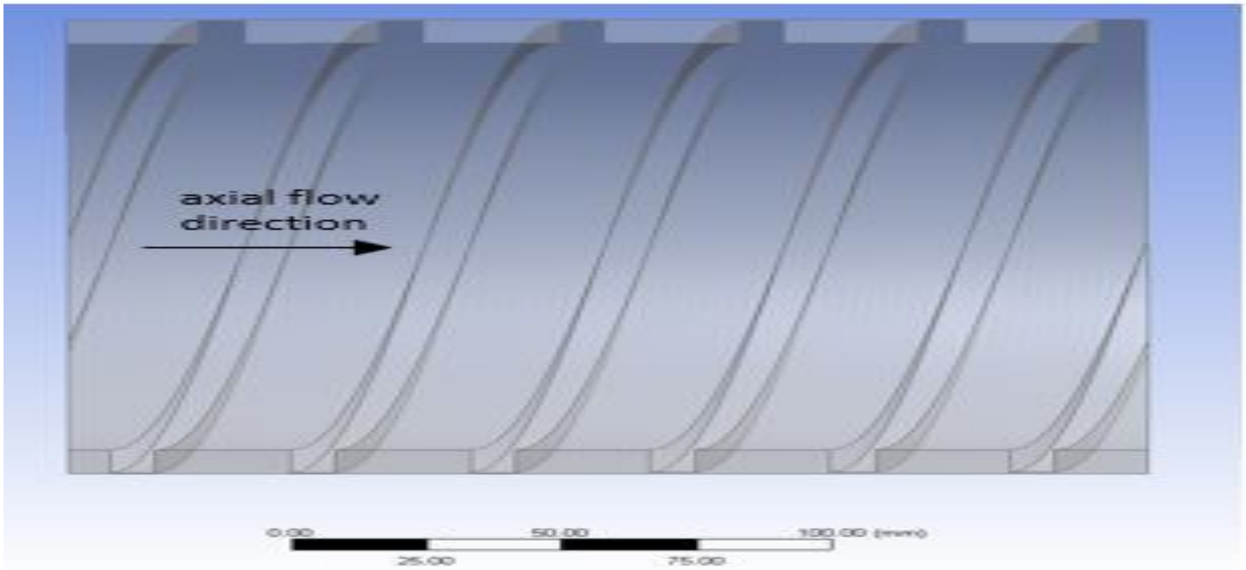

Figure 1: Axial flow direction of a helical groove seal shown on stator surface

Additionally, helical groove seals can resist flow by acting as a pump. The fluid flowing along the groove path is positively displaced back towards the high-pressure region. Essentially, the fluid is pushed back as it tries to escape. This path is shown in Figure 2.

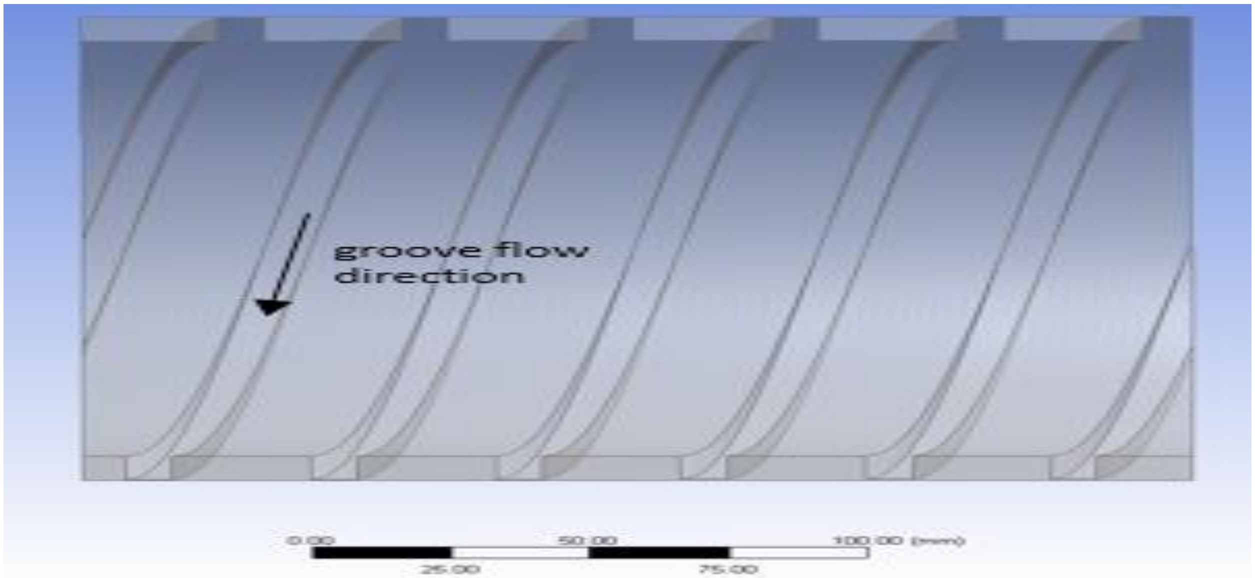

Figure 2: Groove flow direction of a helical groove seal shown on stator surface

Helical groove seals are non-contacting annular seals with continuously cut grooves, like the threads of a screw, cut across the surface of the rotor, the stator or both. Labyrinth seals are non-contacting annular seals with circumferentially cut grooves on the surface of the rotor and/or the stator. Chapter 2 of this thesis describes the methodology used to evaluate the performance of a novel seal design that has helical grooves on one surface and labyrinth grooves on the other. The fluid domain for the two configurations, helical groove rotor and labyrinth stator and helical groove stator and labyrinth rotor, are shown in Figure 3.

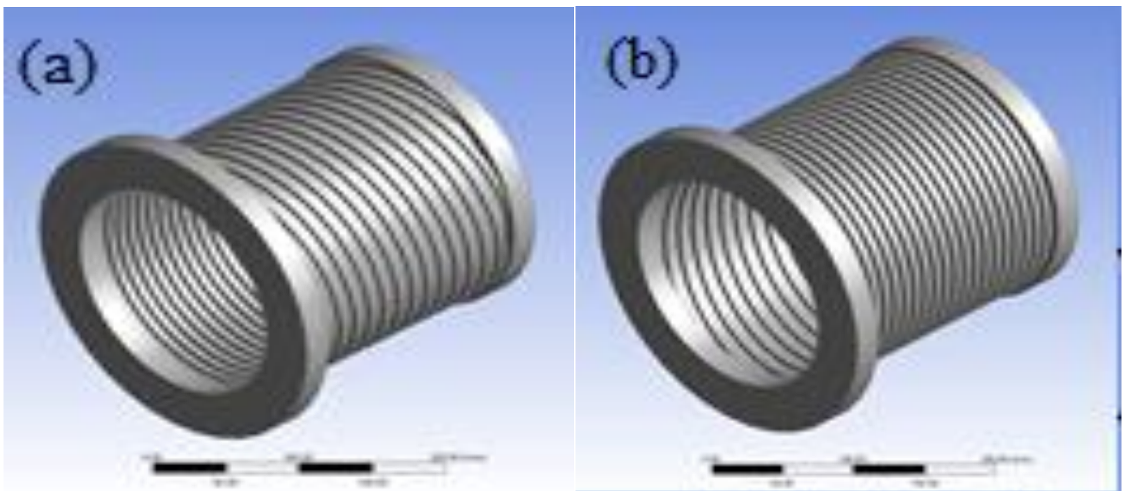

Figure 3: Fluid domain of (a) helical groove stator and labyrinth rotor seal (b) helical groove rotor and labyrinth stator seal

While there are almost no previous studies on mixed helical-labyrinth seals, there has been a lot of research conducted on helical and labyrinth seals over the years. A brief discussion of some of the major works is included since they serve as the basis for the current study on mixed seals. One of the first primary papers on seals and bearing technology was published in 1968 by Anderson and Ludwig [1], where the authors theorize the pumping flow mechanism of helical groove seals. As the pumping of the grooves balances the pressure to be sealed, a liquid-gas interface is established within the seal length, which leads to a pressure gradient from atmospheric at the interface, increasing across the seal length, to the sealed pressure as shown in Figure 4.

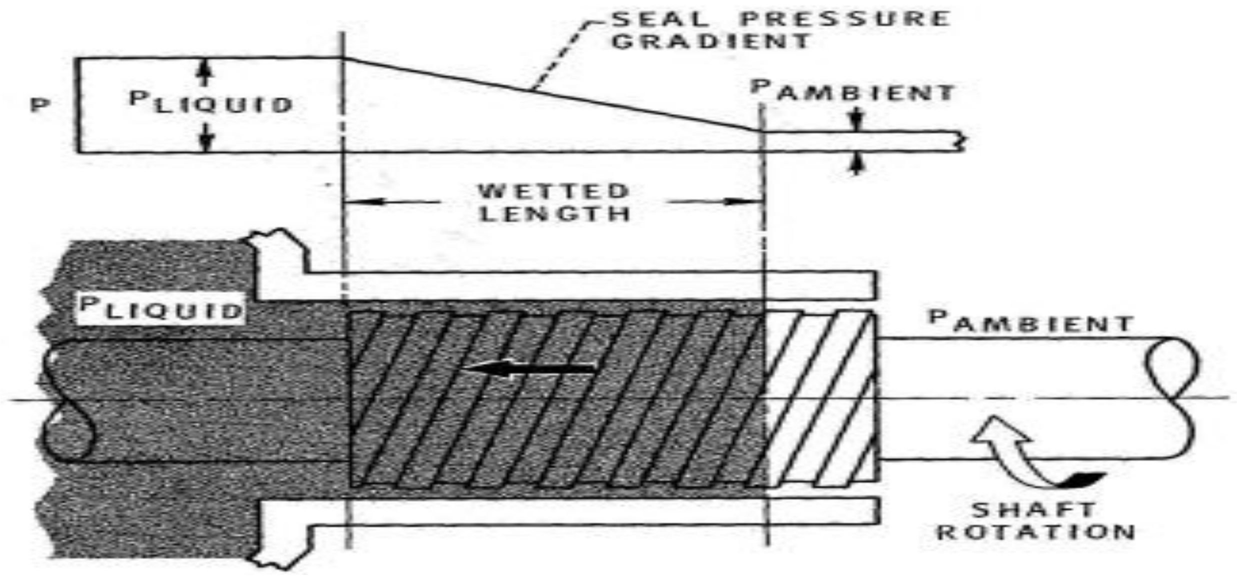

Figure 4: Upstream pumping mechanism of helical groove seal with grooves on the rotor [1]

Other major developments on both helical and labyrinth seals were made in the 1980s primarily by Dr. Dara Childs. More specifically in 1983, through experimental work on helical grooved seals for three different helix or pitch angles and two different clearance values, he discovered their high potential for leakage reduction compared to plain annular seals [2]. In 1987, Kim and Childs [3] conducted analysis for rotordynamic coefficients of helically-grooved turbulent annular seals and theorized that labyrinth seals could possess greater concerns for rotordynamic stability compared to helical seals due to their ability to impart high circumferential velocity on the fluid. In 1990, Childs et al. [4] tested the aforementioned theory through experiments on smooth rotor, helical grooved stator by varying helix angles from zero (labyrinth grooving) to 70 deg. The results showed that helically grooved stator had much lower values of cross-coupled stiffness, the term that contributes to the destabilizing forces on the labyrinth seals, compared to smooth or honeycomb stator seals. That same year, Iwatsubo et al. [5] calculated experimentally the leakage and the dynamic characteristics of five types of spiral grooved seals and an equivalent labyrinth seal design. They found that having grooves on the rotor (as opposed to the stator), while beneficial for leakage reduction can have a worse effect on the rotor stability. The results observed is attributed to the circumferential flow produced by the flow along the groove angle direction that can act as a negative swirl.

While the studies on helical and labyrinth seals date back to several decades and have continued to increase today, this work on mixed grooved seals is based on the most recent computational studies completed by Dr. Cori Watson at the Rotating Machinery and Controls (ROMAC) lab at the University of Virginia. More specifically, the three studies that are referred several times in this thesis are as follows. The first paper looked at optimizing helical groove seals with grooves on both the rotor and stator surfaces, where it was discovered that seals with grooves on both surfaces produced less leakage compared to seals with grooves on just one surface [6]. In the second study, Watson et al. [7] develop an optimal helix angle for helical seals at various pressure differentials, and the optimal seal obtained for a pressure differential of 1 MPa was used for the low pressure case in this study as described in Chapter 4. Finally, the third paper is on the experimental validation of CFD for modeling helical groove seals based on the experiments done by Childs and Iwatsubo in the late 1980s and early 1990s [8]. The report showed that the average error between the computational model and previous experimental work is approximately 3%. Since there are no experimental works done on mixed seals, the analysis done in this thesis was based on this same validation.

In both helical groove and labyrinth seals, leakage is reduced via dispersion of kinetic energy. As the fluid enters the grooves and then exits into the jet stream region in between the grooves, energy is dissipated via turbulent mixing. Helical groove seals also reduce leakage by causing fluid rotation in a direction opposite to the shaft rotation, thus reducing the average axial and circumferential fluid velocity [9]. Helical groove seals are commonly used in pumps because of their ability to sustain higher pressure ratios than other seals [10]. Previous work has shown that the selection of geometric parameters is especially important for helical groove seals because of the wide range of leakage values between different geometries [11]. It has also been shown that seals with grooves on both the rotor and the stator surfaces have lower leakage than seals with grooves on just one surface [6]. In Chapter 3, this claim is further investigated by examining the impact of having two different groove types in the rotating and stationary surfaces of the seal on its leakage. More specifically, an optimal design of a seal, one with minimum leakage, with helical grooves on rotor and labyrinth grooves on the stator or vice-versa is obtained for high pressure applications.

In Chapter 4, the source of the aforementioned leakage reduction is analyzed. This is performed by looking at the effect that the addition of a labyrinth surface has on an optimal helical design in terms of leakage as well as power loss properties of the seals. The source of leakage reduction is investigated by analyzing the circumferential velocity, streamlines of flow, and axial pressure distribution. For both helical and labyrinth seals, the groove profiles on either the rotor or the stator surface create narrower fluid flow lanes which lead to better sealing through flow resistance along the continuous groove [12]. This flow resistance or the pumping effect of the grooves can be correlated to the circumferential velocity and depends on the centrifugal forces and viscous losses as well as the surface geometry. The flow streamlines in the jet stream region suggest a longer helical path for the escaping fluid and the axial pressure distribution indicates kinetic energy dissipation. The impact of various geometric parameters of the seal on leakage and power loss is explored by plotting the regression models generated.

The motivation for this study on mixed seals thus comes from the findings from previous studies where it was discovered that having grooves on both rotor and stator surfaces showed leakage reduction compared to seals with grooves on just one surface [6]. So the paramount objective of this research is to quantify how much better having helical grooves on one surface and labyrinth on the other would be in terms of leakage reduction in both high and low pressure applications compared to the seals that are currently in industry. The author wants to investigate the impact of adding and optimizing labyrinth surface to an already optimal helical seal. Additionally, the goal is also to quantify the relative increase or decrease in power consumption of the machine due to these mixed seals. The positive findings of this work would indicate the benefits of using these mixed seals for leakage reduction at high pressure pumping applications or at low pressures as bearing end seals.

To evaluate these seals, computational fluid dynamic modeling is used. Models of mixed helical groove and labyrinth seals are simulated in ANSYS CFX. The design variables of groove size and angle for each surface are varied through the design space. The results are compared with the helical groove seal with grooves on the stator analyzed in the literature [11]. In this study, the author derives a regression model that can be used to predict the performance of other mixed helical groove and labyrinth seals within the design space. This multifactor quadratic regression model helps determine the influence each design parameter has on the leakage and power loss performance and enables better understanding of the benefits and physical mechanisms of these seals.

CHAPTER 2: METHODOLOGY

This chapter considers the process utilized to analyze the mixed seals introduced in Chapter 1. First, the discussion of the seals' geometric models and operating conditions is included. Next, the numerical ANSYS model, boundary conditions, and the advantage of using a sector model are examined. Finally, the chapter concludes with the selection of the best mesh size for both high and low pressure cases.

Geometric Model and Constraints

The spacing of the grooves, s, is determined by the helix angle, α, groove width, w, and number of grooves, N. It can be solved by using:

$$\frac{N(s+w)}{2\pi \cdot R_S} = \tan \alpha \qquad (1)$$

This function is determined by calculating the length of the seal using the groove parameters and dividing by the circumference to find the angle. The groove width and spacing are measured as the lengths in the axial direction as shown in Figure 5. For helical grooves, the helix angle is measured from the circumferential direction. The geometric constraint necessary to ensure that these helical grooves do not overlap is found by solving for groove spacing in Equation 1.

$$\frac{2\pi \cdot R_S \tan \alpha}{N} - w > 0 \qquad (2)$$

Similarly, in order for the labyrinth grooves to not overlap, an individual groove width multiplied by the total number of grooves has to be less than the total length of the seal, L, as shown in Equation 3.

$$wN < L \qquad (3)$$

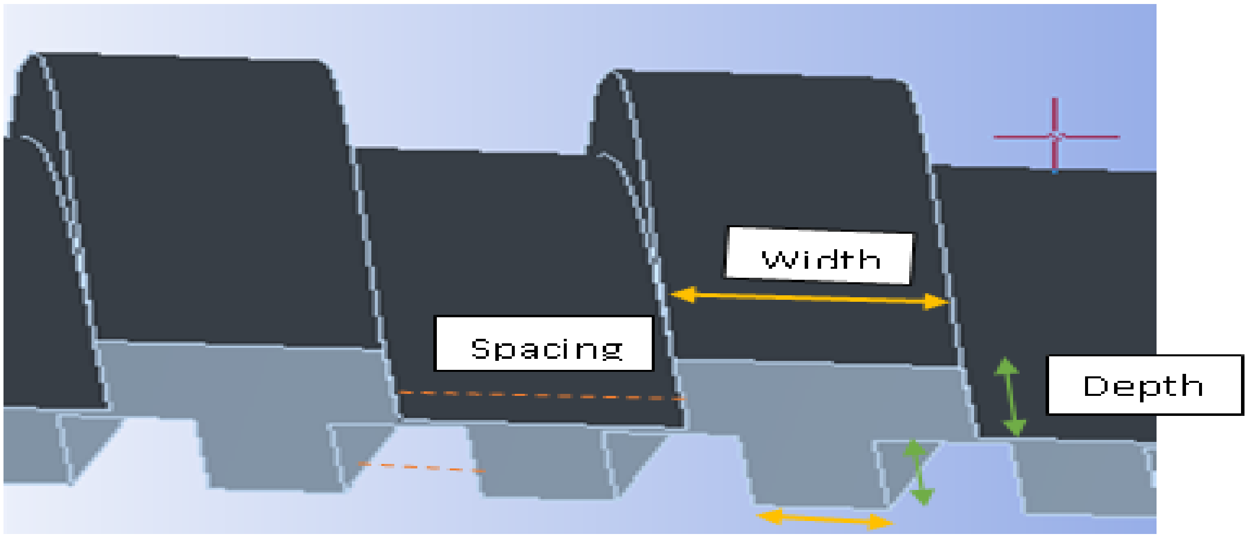

Figure 5: Measurement of groove width, depth and spacing

Operating Conditions

The operating conditions used here are determined from liquid pump operating conditions and are summarized in Table 1. The values of these conditions are taken from the manufacturers and are selected based on what were believed to be the most applicable for industrial use. The design parameters varied include labyrinth width, labyrinth depth, number of labyrinth grooves, helical groove width, helical groove depth, and helix angle. For high pressure application, all six parameters were varied and the optimized seal is identified as explained in Chapter 3. On the other hand, for low pressure case, where the inlet pressure is set at 1 MPa, the optimized helical surface is kept constant and only the labyrinth parameters are varied as discussed in Chapter 4. The groove size is defined by the groove width and depth, which are assumed equal based on the optimal seal from [7].

Seal Length, L	***200 mm***
Rotor Radius, R	***100 mm***
Clearance, C_r	***0.5 mm***
Rotor Speed, Ω	***5000 rpm***
Inlet Pressure, P_i	***25 MPa***
Outlet Pressure, P_o	***0 MPa***

Table 1: Operating conditions for high pressure liquid pump

Numerical Model and Boundary Conditions

As mentioned in Chapter 1, the analysis was conducted using ANSYS CFX, which solves the Reynolds Averaged Navier Stokes Equations (RANS). The fluid studied is water at 25° C with an isothermal energy model. Turbulence is modeled using $\kappa - \varepsilon$ model, which provides a general description of turbulence by means of two transport partial differential equations including turbulent kinetic energy (k) and turbulent dissipation (ε). It focuses on the mechanisms that affect the turbulent kinetic energy under the assumption that turbulent viscosity is isotropic.

Most Computational Fluid Dynamics (CFD) studies of rotating machinery components use the two equation models to model turbulence, primarily Shear Stress Transport (SST) or k-epsilon. In order to select the appropriate model, the boundary layers and a non-dimensional quantity known as y+ need to be examined for the case under investigation. As can be observed from Figure 6, a typical wall-bounded flow consists of three main layers that separate the boundary from the free stream flow region. These layers are the viscous sublayer, the buffer layer, and the log-law region.

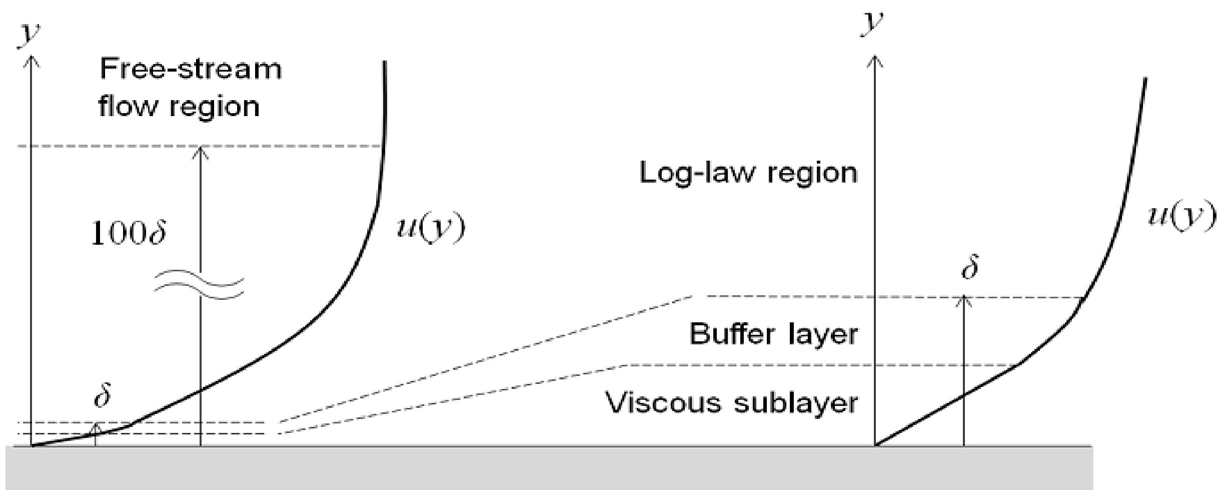

Figure 6: Boundary sub-layers for a wall bounded flow

The distance from the wall to each of these sublayers is called the y+. This distance is often non-dimensionalized in the following way:

$$y^+ = \frac{u_* y}{v}\,, \qquad (4)$$

where u_* is the friction velocity, y is the distance from the wall, and v is the local kinematic viscosity. Y+ is typically used in reference to a mesh, where y is the first layer height. Each turbulence model has an acceptable range for mesh y+. According to von Karman Law of the Wall, the viscous layer lies up to a y+ of 5, the buffer layer between 5 and 30, and log-law region is at a y+ of above 30 [13]. The SST turbulence model requires a mesh y+, from the first layer thickness, below the viscous layer, while the $\kappa - \varepsilon$ model requires a mesh y+ above the buffer layer. In order to account for all three boundary sub-layers in the analysis, the $\kappa - \varepsilon$ model was selected for the purpose of this research.

Each simulation is considered to have converged when it reached a root mean square residual of 10^{-5}. Medium intensity turbulence (between 1-5%) is selected at the inlet as is typically done for modeling flows in seals. Homogeneous boundary conditions are considered because of the inclusion of the upstream region in the model. The inlet pressure is specified as total pressure and the outlet boundary condition is the average static pressure. In order to prevent mesh deformation, the helical surface is modeled as a stationary wall regardless of whether it is on the stator or the rotor. For the helical stator and labyrinth rotor configuration, the domain is modeled in a stationary reference frame with the rotor moving at the rotational speed. For the helical rotor and labyrinth stator configuration, the domain is modeled in a reference frame rotating at the rotor speed and the stator surface is set to counter-rotate at the rotational speed. The inclusion of inlet and outlet regions as shown in Figure 7 allows the flow to recirculate before exiting the outlet and prevents the need to calculate pre-swirl at the entrance to the seal. The flow, therefore, is assumed to be normal to the boundary at the inlet.

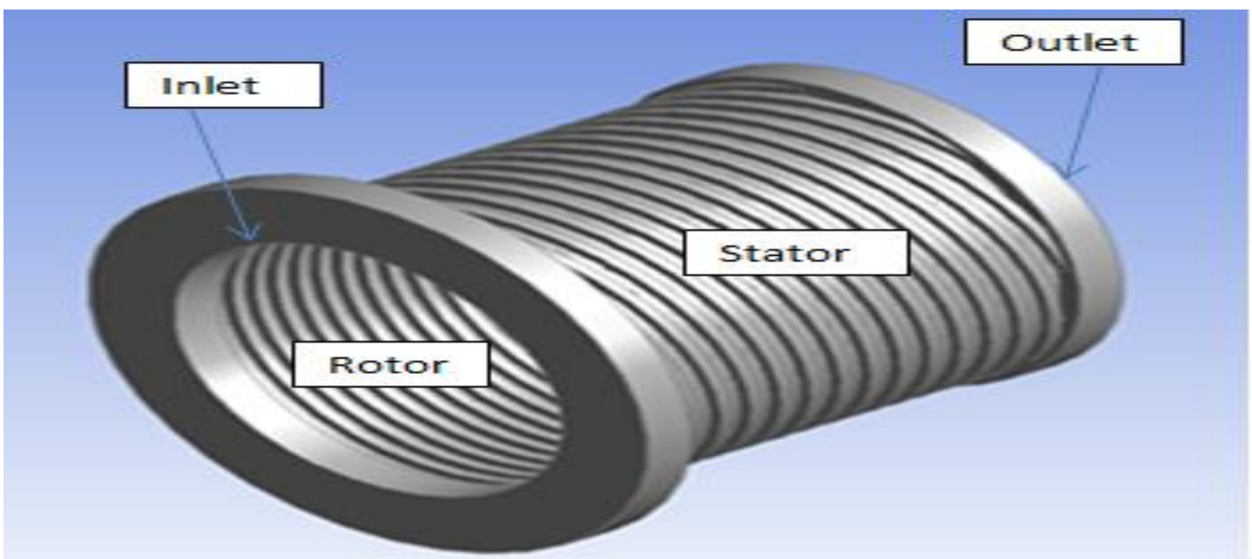

Figure 7: Helical stator labyrinth rotor seal with inlet and outlet regions

Sector Model

The full 360 degrees model of the seal was broken down into a sector in order to reduce the number of mesh elements required for computation and therefore the total computational time needed to run the simulation. The sector uses periodic boundary conditions with a flux conservative interface to model the whole seal with just a part. Figure 8 shows a sector of a helical groove seal used in this study.

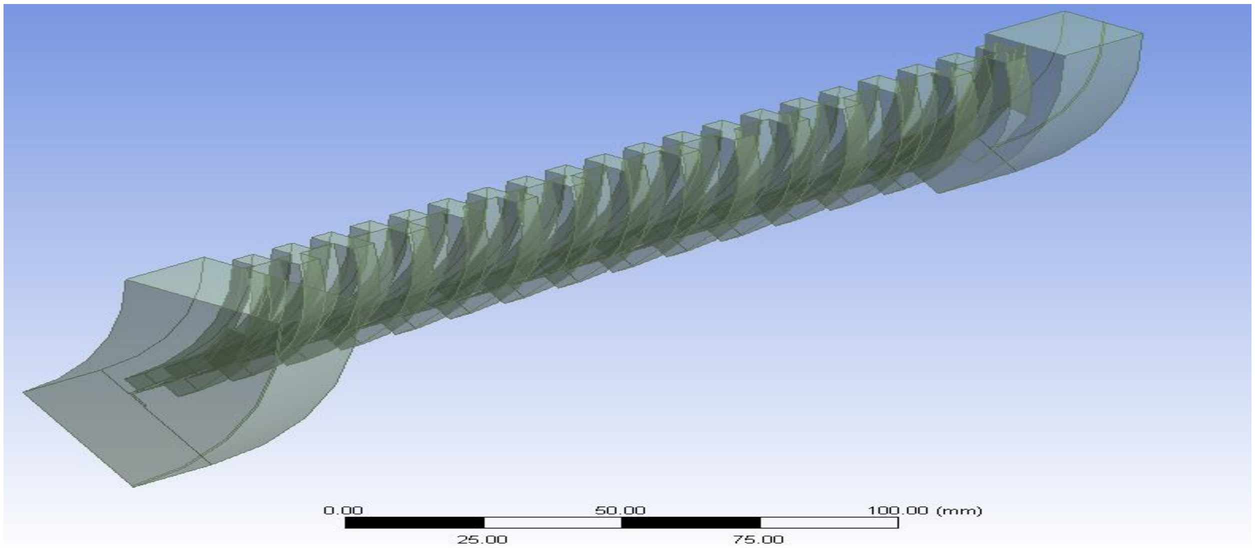

Figure 8: Sector model of helical groove seal

In order to highlight the benefits of using a sector model, the computational time for an 18 groove helical seal versus the sector size is plotted in Figure 9. It can clearly be observed that the geometric size of the seal and computational time have a linearly inverse relationship. For helical groove seals, the sector size must be a divisor of the number of grooves. For example, this 18 groove helical seal could be in sectors of a half, a third, a sixth, a ninth, or an eighteenth, i.e. 180^0, 120^0, 60^0, 40^0 or 20^0 respectively. For other sector sizes, the interfaces at the left and right side of the sector do not line up and rotational periodicity is not maintained. The effect of sector size on leakage performance for helical groove seals was explored by Watson et al. in [8]. Labyrinth seals are circumferentially symmetric and therefore can be cut into sectors of any size.

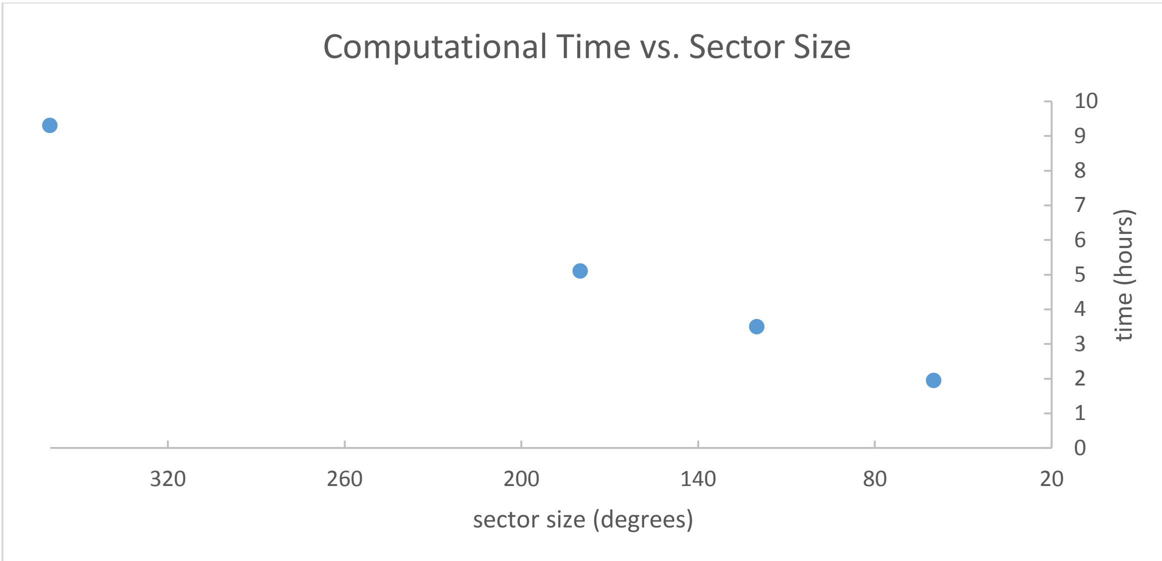

Figure 9: Computational time versus sector size for an 18-groove helical seal

Mesh Independence Study: High Pressure Case

A mesh independence study was performed for the baseline geometry shown in Figure 8. Since the helical surface had 8 grooves, the smallest possible sector for the baseline geometry is used, which is 1/8th or a 45^{0} section. The mesh of the baseline seal is shown in Figure 10.

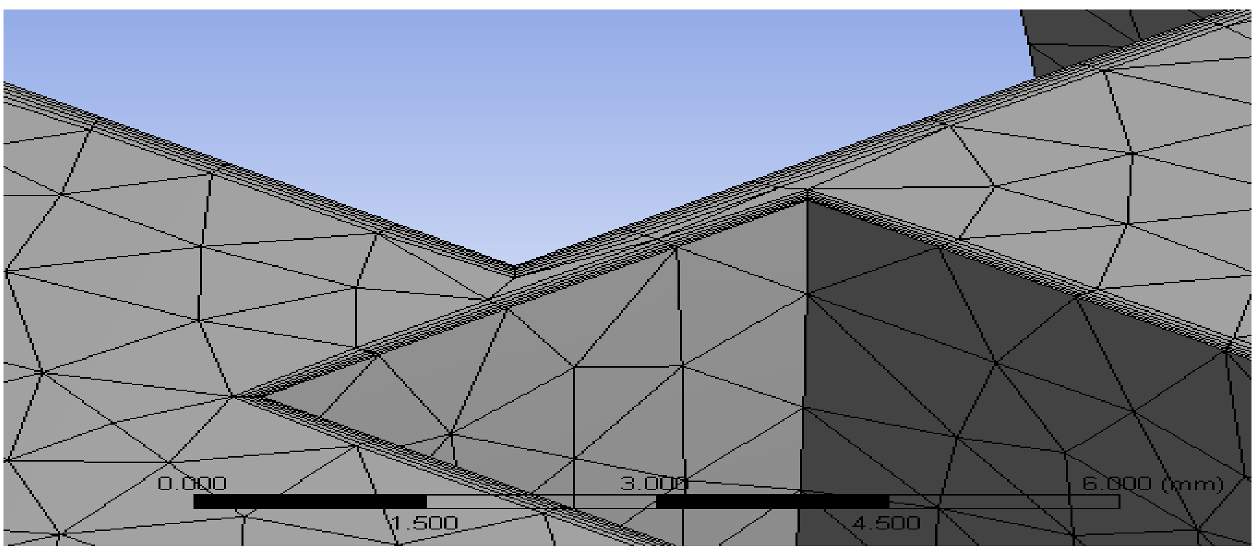

Figure 10: Mesh used based on boundary layers and mesh independence

The results of the mesh study are summarized in Table 2.

Mesh size	Leakage	Error
0.338 million	2.8824	13.99%
0.416 million	3.2647	2.587%
0.547 million	3.2875	1.907%
0.749 million	3.3514	-------------

Table 2: Mesh independence study results

From Table 2, it can be seen that the percent difference on the leakage values obtained for the mesh size of 0.42 and 0.55 million elements is 2.5%. A mesh coarser than that would result in significant error in leakage, thus 0.42 million elements are deemed sufficient for this case. The rotor y+ value is 79 and the stator y+ value is 58, which matches the k-ε assumption of the average y+ value of approximately 70. The boundary layers are shown in Figure 11. The wall surfaces have two to three boundary layer elements accounting for 30% of the clearance thickness.

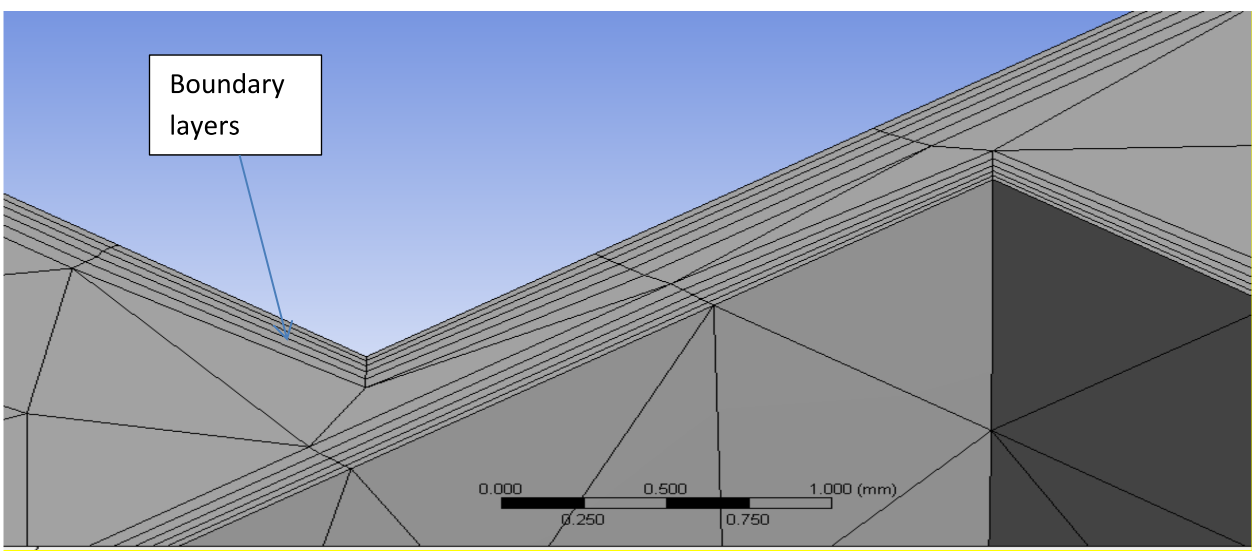

Figure 11: Boundary layers added to accurately capture near-wall effects

In order to ensure that the finer resolution of the boundary layer does not have significant influence on the solution, a mesh with a smooth transition in element size and a growth rate of 1.2 was also investigated as seen in Figure 12 below. With those parameters, the error in the baseline case was 1.4% which is within the error of the mesh independence. This mesh was not used for other cases as it had three times as many elements and thus would require significantly more simulation time.

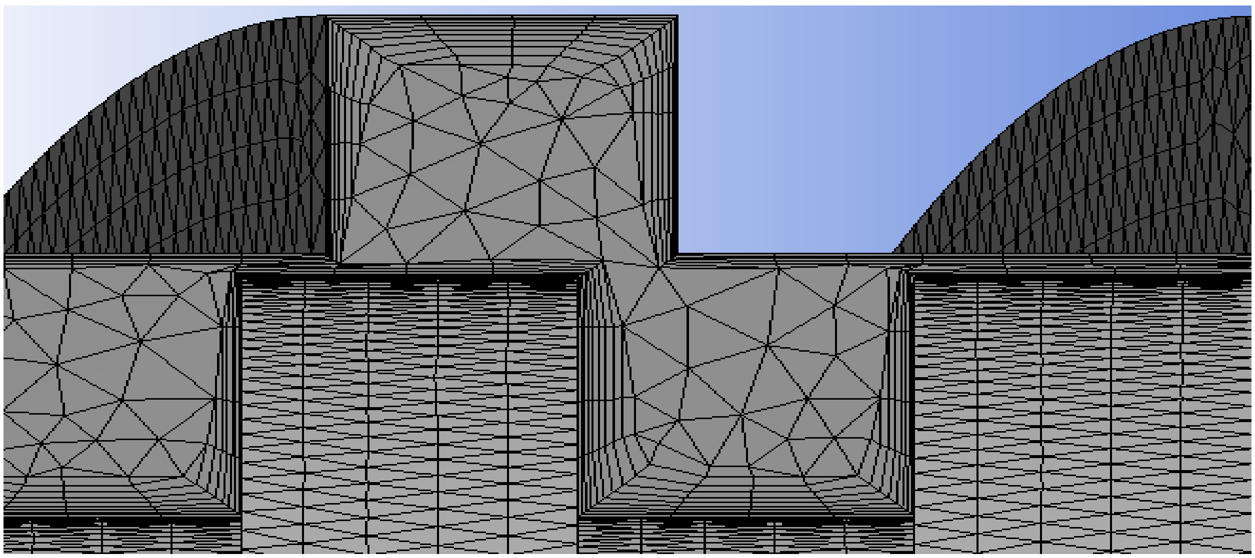

Figure 12: Finer mesh with smooth transition and growth rate of 1.2

MESH INDEPENDENCE: LOW PRESSURE CASE

In order to ensure that the results obtained were unaffected by mesh discretization, a mesh independence study was once again conducted on the 1/13th or 27.7 degrees sector model of the seal as shown in Figure 14. This sector size was determined based on the fact that the optimal helical surface used for the low pressure case had 13 helical grooves, which was based on the optimal helical design discovered for a pressure of 1 MPa in [7]. To briefly summarize the results obtained in [7], the plot of leakage versus helix angle at 1 MPa is shown in Figure 13 below.

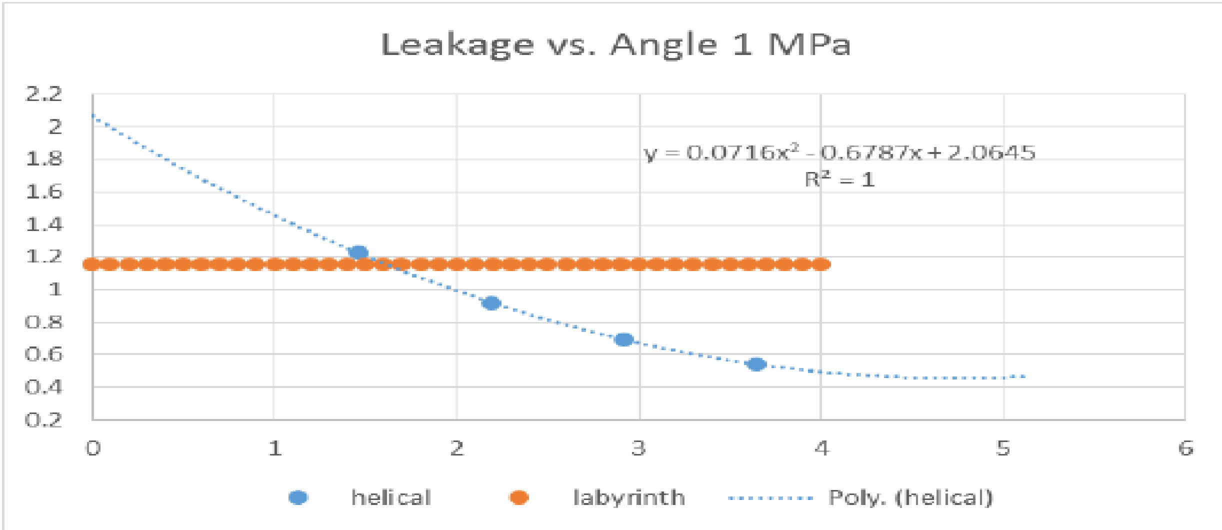

Figure 13: Leakage versus helix angle for 1 MPa pressure differential as obtained from [7]

The horizontal dotted line is the leakage obtained for labyrinth seal while the curve shows a decrease in leakage with an increase in helix angle up until about an angle of 4° where the curve begins to flatten. By approximating the lowest leakage value from the plot as 0.45, the equation of the curve can be solved to determine the optimal helix angle as follows:

$$y = 0.0716x^2 - 0.6787x + 2.0645$$

$$0.45 = 0.0716x^2 - 0.6787x + 2.0645$$

$$x \approx 4.7$$

By setting, y = 0.45 kg/s, x is obtained to be approximately 4.7°. Thus, using this optimal angle to solve for equation (1), one can determine the total number of grooves on the optimal helical surface. This calculation is demonstrated below:

$$N * \frac{w + s}{2 * pi * R_s} = \tan(\alpha)$$

$$\frac{N(2 + 2)mm}{2 * 3.1415 * 100.5\ mm} = \tan(4.7°)$$

$$N \approx 13$$

Thus, the mesh independence study was conducted on the 1/13th sector of the seal. The mesh on the baseline seal with the constant helical surface is shown in the figure below.

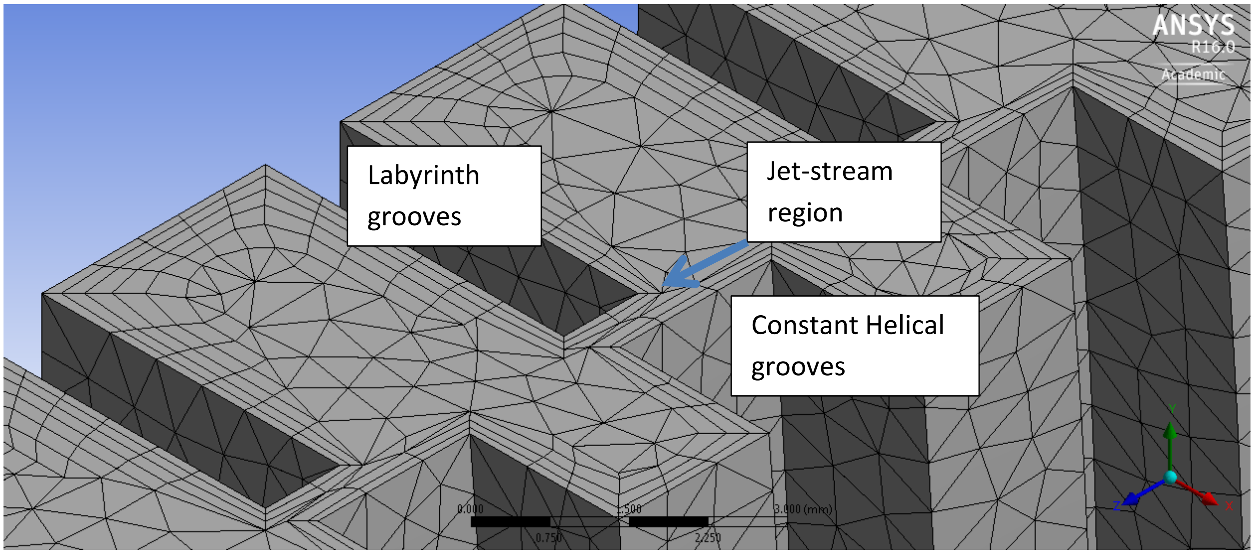

Figure 14: Mesh of the baseline sector seal model based on mesh independence

The results of the mesh independence study are summarized in Table 3 below:

Element size (mm)	Mesh size (elements)	Sector Leakage (kg/s)	% diff	Power loss (kW)	% diff
1.5	524307	-0.0394	27.960	-1.595	10.579
0.95	982487	-0.0506	7.371	-1.649	7.514
0.85	1286111	-0.0491	10.127	-1.669	6.388
0.78	1635160	-0.0516	5.632	-1.715	3.828
0.65	2184955	-0.0536	1.854	-1.755	1.572
0.55	3049067	-0.0546		-1.783	

Table 3: Mesh independence for leakage and power loss

The average rotor y+ value for the baseline case is 94 and the average stator y+ value is 95, which fall within the range of y+ values for the k-epsilon assumption of 30-100 [14].The mesh with the element size of 0.65 mm or 2.18 million elements is used in this study since it has less than 2% error as illustrated in Table 3. The mesh has 10 boundary layers that were added to ensure accurate results for power loss calculations. The boundary layers are shown in Figure 15.

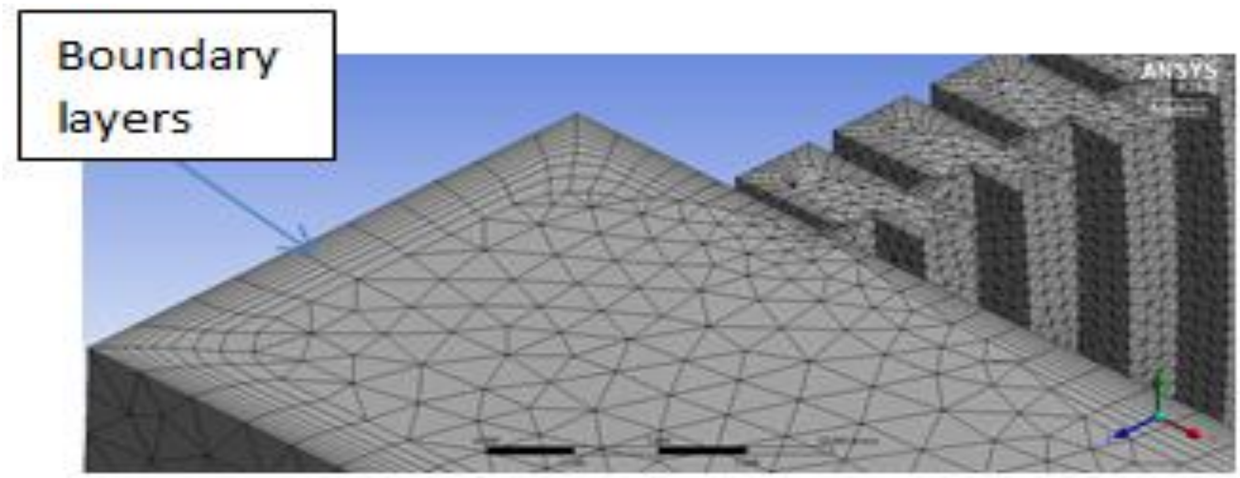

Figure 15: Boundary layers added to accurately capture the near-wall effects

The mesh used also had smooth transition in element size and a growth rate of 1.2 which further ensured the accuracy of the solution it produced for power loss as shown in [7].

CHAPTER 3: RESULTS – HIGH PRESSURE

This chapter presents the data analysis and results obtained for the performance of mixed helical labyrinth seals at a high operating pressure of 25 MPa. A series of design parameters were simulated and an optimal seal with the best leakage performance was obtained. Using a backward regression model, various surface response plots were developed to fully understand the impact of each design parameter on fluid leakage. The findings of this particular study were presented at ASME Turbo Expo 2017 in Charlotte, NC [15].

Design of Experiments

The design variables in this study are labyrinth width, labyrinth depth, number of labyrinth grooves, helical groove width, helical groove depth, and helix angle. Ranges of values for these parameters are given in Table 4.

Labyrinth width (lw)	Labyrinth depth (ld)	Number of labyrinth grooves (nlg)
3 mm	3 mm	10
5 mm	5 mm	20
7 mm	7 mm	30
9 mm	9 mm	40
Helical width (hw)	Helical depth (hd)	Helix angle (ha)
3 mm	3 mm	6°
5 mm	5 mm	10°
7 mm	7 mm	15°
9 mm	9 mm	30°

Table 4: Range of values for design parameters

In total, there are 6^4 or 1296 combinations of these design parameters for each of the two design configurations, namely helical stator labyrinth rotor and helical rotor and labyrinth stator. The regression analysis performed contains 28 coefficients so a minimum of 28 simulations are needed for each configuration. In order to get an accurate estimate of the statistical significance of that regression model, twice that number of simulations need to be run. The 56 designs for each configuration are chosen starting with the baseline design, which has labyrinth width, labyrinth depth, helical width, and helical depth of 5 mm each, 20 labyrinth grooves and a helix angle of 10^0. From the baseline design, additional simulations are selected using a Kennard-Stone algorithm. The Kennard-Stone algorithm selects designs in a way to maximize the dissemination of designs in the design space [16]. Each new design is selected based on being the maximum total distance from all of the previous designs simulated. For example, the second design simulated is the one furthest from the baseline design. The third design is the one furthest from both of the previous two and so on until all of the designs are selected. Designs that violate the physical constraints in equations (2) and (3) are removed from the data set.

Data Analysis

Based on the 112 simulations, two multifactor quadratic regression models can be fitted to the leakage data. The 6 variables produce 6 quadratic terms, 6 linear terms, 15 cross terms and the constant term. The 28 coefficients of the design variables are shown in Table 5 for the helical groove rotor and labyrinth stator configuration.

	Coefficients	*Standard Error*	*t Stat*	*P-value*
(Intercept)	-0.56462	0.42418	-1.3311	0.19429
lw	0.08842	0.12067	0.73277	0.47002
ld	0.030436	0.085026	0.35796	0.72316
nlg	-0.00023121	0.019807	-0.011673	0.99077
hw	0.44067	0.11192	3.9373	0.00052237
hd	0.082513	0.19254	0.42854	0.67165
ha	0.08504	0.026646	3.1915	0.0035751
lw^2	0.003554	0.0092679	0.38347	0.70437
ld^2	-0.0014413	0.0072447	-0.19895	0.84379
nlg^2	-0.00019672	0.00033325	-0.59031	0.55989
hw^2	-0.027974	0.01226	-2.2817	0.030613
hd^2	0.0022259	0.022487	0.098987	0.92188
ha^2	-0.0016788	0.00070982	-2.3651	0.025468
lw*ld	-0.0013625	0.0022387	-0.60862	0.54786
lw*nlg	-0.0010147	0.0017547	-0.57827	0.56787
lw*hw	-0.0093401	0.0027939	-3.343	0.00244
lw*hd	-0.008512	0.00845	-1.0073	0.32272
lw*ha	-0.0013126	0.00064527	-2.0342	0.051864
ld*nlg	-0.00024636	0.00045317	-0.54363	0.59115
ld*hw	-0.00037741	0.0023488	-0.16068	0.87354
ld*hd	-0.00066587	0.0023955	-0.27797	0.78316
ld*ha	5.3955e-05	0.0005667	0.095209	0.92485
nlg*hw	0.00032787	0.00056751	0.57774	0.56823
nlg*hd	0.0011333	0.00067996	1.6668	0.10712
nlg*ha	-0.0006715	0.00013669	-4.9124	3.8544e-05
hw*hd	0.039828	0.0029456	13.521	1.5429e-13
hw*ha	0.002056	0.00181	1.1359	0.26599
hd*ha	0.0048456	0.00071699	6.7583	2.9467e-07

Table 5: Initial coefficients of regression model for helical groove rotor and labyrinth stator configuration

Similarly, the 28 coefficients for the helical groove stator and labyrinth rotor configuration are shown in Table 6.

	Coefficients	*Standard Error*	*t Stat*	*P-value*
(Intercept)	-1.8175	0.91118	-1.9946	0.056267
lw	-0.020987	0.2592	-0.080967	0.93607
ld	0.080664	0.18265	0.44164	0.66226
nlg	0.078368	0.042547	1.8419	0.076499
hw	0.72315	0.24043	3.0078	0.0056368
hd	0.14148	0.41361	0.34207	0.73494
ha	-0.13552	0.057239	-2.3676	0.025323
lw^2	0.0096935	0.019909	0.4869	0.63026
ld^2	-0.0083406	0.015563	-0.53594	0.59639
nlg^2	-0.001216	0.00071585	-1.6986	0.10089
hw^2	-0.036932	0.026336	-1.4023	0.17221
hd^2	-0.0017714	0.048304	-0.036671	0.97102
ha^2	0.003093	0.0015248	2.0285	0.052477
lw*ld	0.0017215	0.0048089	0.35798	0.72314
lw*nlg	0.0046422	0.0037694	1.2315	0.22874
lw*hw	-0.016108	0.0060017	-2.684	0.012276
lw*hd	-0.010992	0.018152	-0.60554	0.54988
lw*ha	0.0025162	0.0013861	1.8153	0.080601
ld*nlg	0.00073759	0.00097346	0.7577	0.45519
ld*hw	0.0060249	0.0050456	1.1941	0.24283
ld*hd	-0.0024322	0.0051458	-0.47265	0.64026
ld*ha	-0.0022291	0.0012173	-1.8311	0.078144
nlg*hw	-0.0035997	0.0012191	-2.9528	0.0064482
nlg*hd	-0.0019539	0.0014606	-1.3377	0.19216
nlg*ha	0.00040822	0.00029362	1.3903	0.1758
hw*hd	0.043763	0.0063274	6.9164	1.9685e-07
hw*ha	-0.002969	0.0038882	-0.76358	0.45174
hd*ha	0.0079337	0.0015402	5.1512	2.0292e-05

Table 6: Initial coefficients of regression model for helical groove stator and labyrinth rotor configuration

The t-statistic is calculated as the ratio of the coefficient to its error and that value is compared against a t-table to find the corresponding p-value. Terms with p-values less than 0.10 are considered statistically significant. Backward regression can be used to remove statistically insignificant terms from the regression model [17]. In backward regression, the term with the highest p-value or least significance is removed from the model. Then, a new regression model is calculated based on the remaining 27 terms. This is repeated until all the remaining coefficients have p-values of less than 0.10. The final coefficients for the helical groove rotor and labyrinth stator configuration are given in Table 7 while the coefficients for the helical groove stator and labyrinth rotor are in Table 8.

	Coefficients	*Standard Error*	*t Stat*	*P-value*
hw	0.44067	0.071584	5.1374	7.6335e-06
hd	0.10555	0.023959	4.4055	7.6924e-05
ha	0.094475	0.02136	4.4231	7.2851e-05
lw^2	0.0098459	0.0011892	8.2795	3.3171e-10
nlg^2	-0.00026353	6.8189e-05	-3.8646	0.00039881
hw^2	-0.016335	0.0061899	-2.639	0.011793
ha^2	-0.0017615	0.00058748	-2.9985	0.0046488
lw*hw	-0.010133	0.0021271	-4.7639	2.5049e-05
lw*hd	-0.0085674	0.0023592	-3.6315	0.00079207
lw*ha	-0.0013231	0.00053315	-2.4817	0.017374
nlg*hd	0.0010431	0.00057084	1.8274	0.075114
nlg*ha	-0.00063302	0.00010066	-6.2888	1.8559e-07
hw*hd	0.039971	0.0025464	15.697	1.0744e-18
hd*ha	0.0047794	0.00061147	7.8162	1.4054e-09

Table 7: Final coefficients of regression model for helical groove rotor and labyrinth stator configuration

	Coefficients	*Standard Error*	*t Stat*	*P-value*
nlg	0.1109	0.024774	4.4764	5.7125e-05
hw	0.82284	0.16031	5.1326	6.9135e-06
ha	-0.13679	0.0482	-2.838	0.0069626
lw^2	0.010249	0.0021028	4.8738	1.6021e-05
nlg^2	-0.0016129	0.00049479	-3.2599	0.0022138
hw^2	-0. 052776	0.013921	-3.7912	0.00047305
ha^2	0.0032281	0.0013533	2.3854	0.021649
lw*hw	-0.011141	0.0046082	-2.4176	0.020042
ld*ha	-0.0013038	0.00046487	-2.8046	0.0075978
nlg*hw	-0.0027284	0.00093592	-2.9152	0.0056802
hw*hd	0.043541	0.0052036	8.3675	1.7276e-10
hd*ha	0.0083155	0.0012589	6.6052	5.3506e-08

Table 8: Final coefficients of regression model for helical groove stator and labyrinth rotor configuration

The R^2 value for the regression model for the helical groove rotor and labyrinth stator model is 0.998, i.e. 99.8% of the variation in leakage can be explained by the regression model. Typically, anything above 0.90 for R^2 is considered a good fit. The final regression model for the helical groove rotor and labyrinth stator configuration is

$$\frac{\dot{m}}{8} \approx 0.3678 * hw + 0.1056 * hd + 0.09448 * ha + 0.009846 * lw^2 - 0.0002635 * nlg^2 - 0.01634 * hw^2 - 0.001762 * ha^2 - 0.010133 * (lw * hw) - 0.0085674 * (lw * hd) - 0.0013231 * (lw * ha) + 0.0010431 * (nlg * hd) - 0.00063302 * (nlg * ha) + 0.039971 * (hw * hd) + 0.0047794 * (hd * ha)$$

(5)

Similarly, the final regression model for helical groove stator and labyrinth rotor configuration is

$$\frac{\dot{m}}{8} \approx 0.1109 * \mathrm{nlg} + 0.82284 * \mathrm{hw} - 0.13679 * \mathrm{ha} + 0.010249 * \mathrm{lw}^2 - 0.0016129 * \mathrm{nlg}^2 - 0.052776 * \mathrm{hw}^2 + 0.0032281 * \mathrm{ha}^2 - 0.011141 * (\mathrm{lw} * \mathrm{hw}) - 0.0013038 * (\mathrm{ld} * \mathrm{ha}) - 0.0027284 * (\mathrm{nlg} * \mathrm{hw}) + 0.043542 * (\mathrm{hw} * \mathrm{hd}) + 0.0083155 * (\mathrm{hd} * \mathrm{ha}) ,$$

(6)

where the R^2 value in this case is 0.986.

Discussion

Response surfaces can be plotted based on both of these regression models. The plot of leakage versus helical width and labyrinth width is shown in Figure 16 for the configuration with helical grooves on the rotor and labyrinth grooves on the stator.

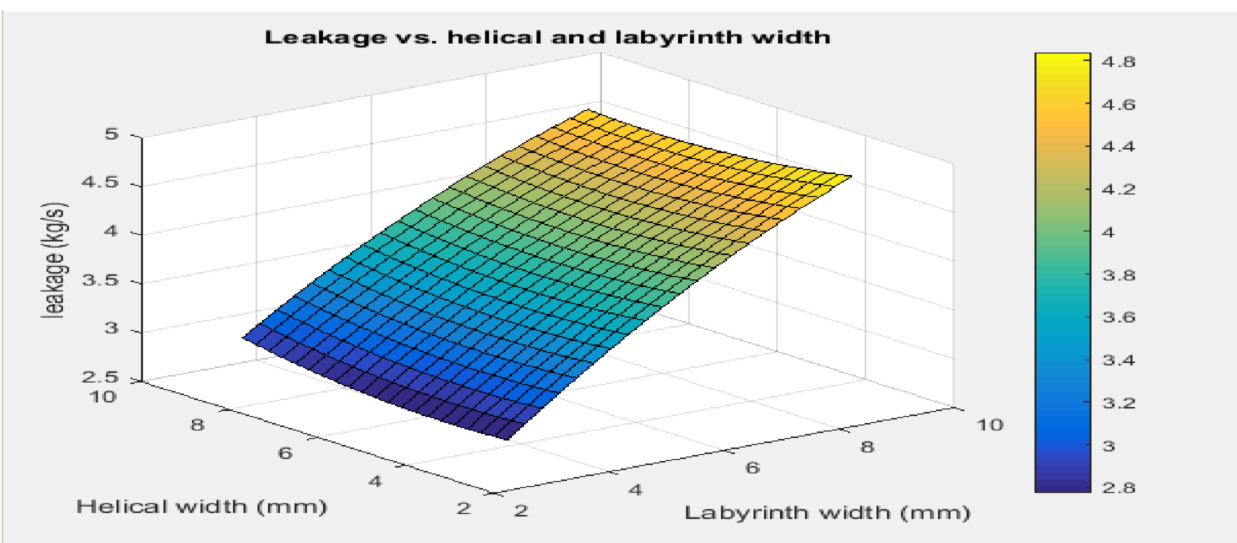

Figure 16: Leakage versus labyrinth width and helical width for helical groove rotor and labyrinth stator configuration

Leakage is substantially reduced by decreasing the labyrinth width, but there are only small improvements from decreasing the helical width. The same variables are plotted for the configuration with helical grooves on the stator and labyrinth grooves on the rotor in Figure 17.

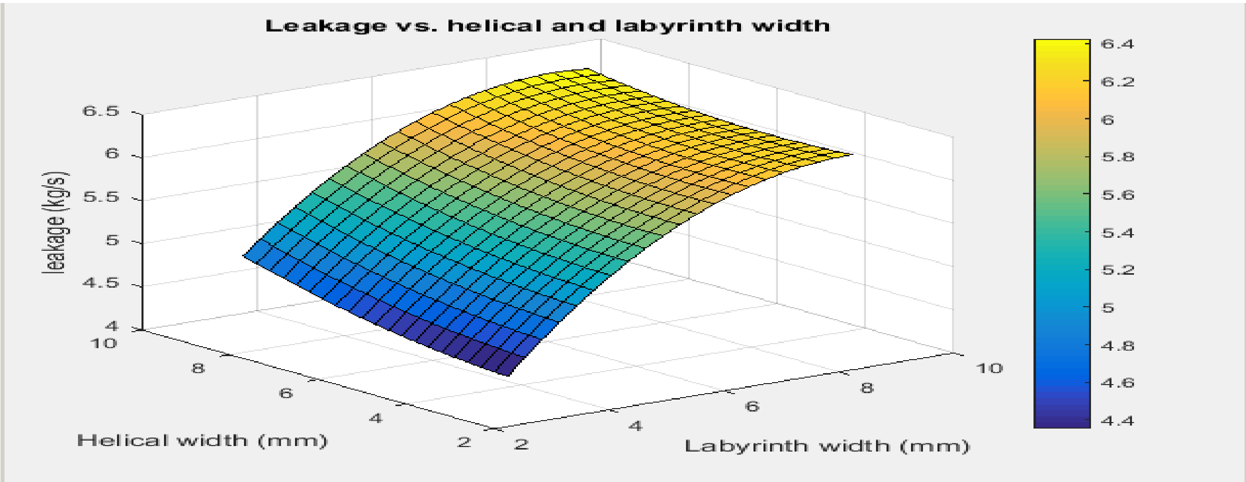

Figure 17: Leakage versus labyrinth width and helical width for helical groove stator and labyrinth rotor configuration

The same general trend is seen here again. The leakage of the helical groove rotor and labyrinth stator seals is plotted versus helical width and helical depth in Figure 18.

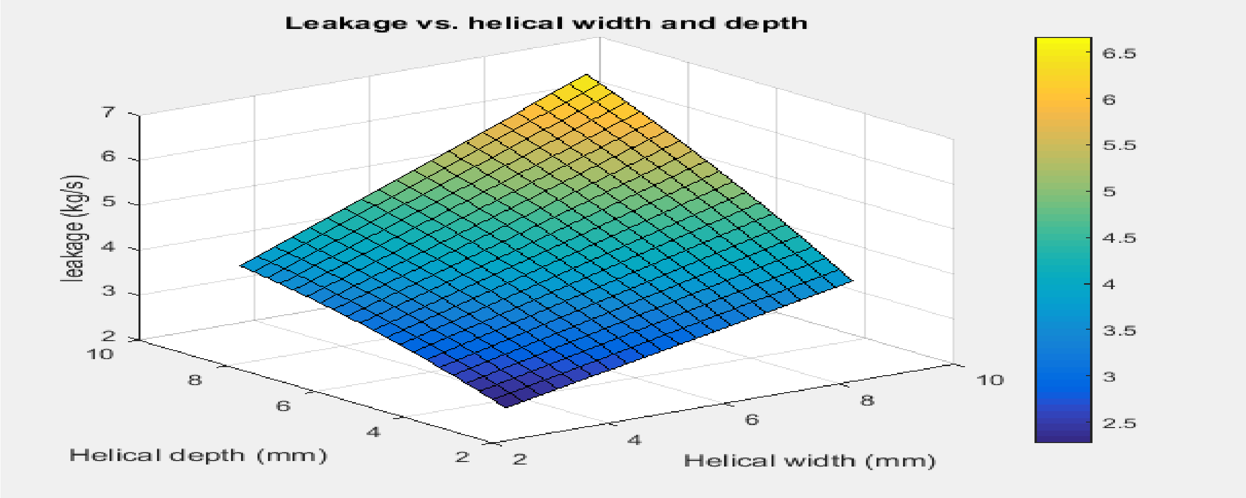

Figure 18: Leakage versus helical depth and width for helical groove rotor and labyrinth stator configuration

When helical width is varied with helical depth, it can be seen that increasing the overall size of the helical groove increases leakage. This is the anticipated outcome since an increase in the overall groove size leads to an increase in the amount of fluid able to escape out of the grooves. This is related to the second to last term, (hw x hd), in the regression model. A similar trend can be observed for the helical groove stator and labyrinth rotor configuration in Figure 19.

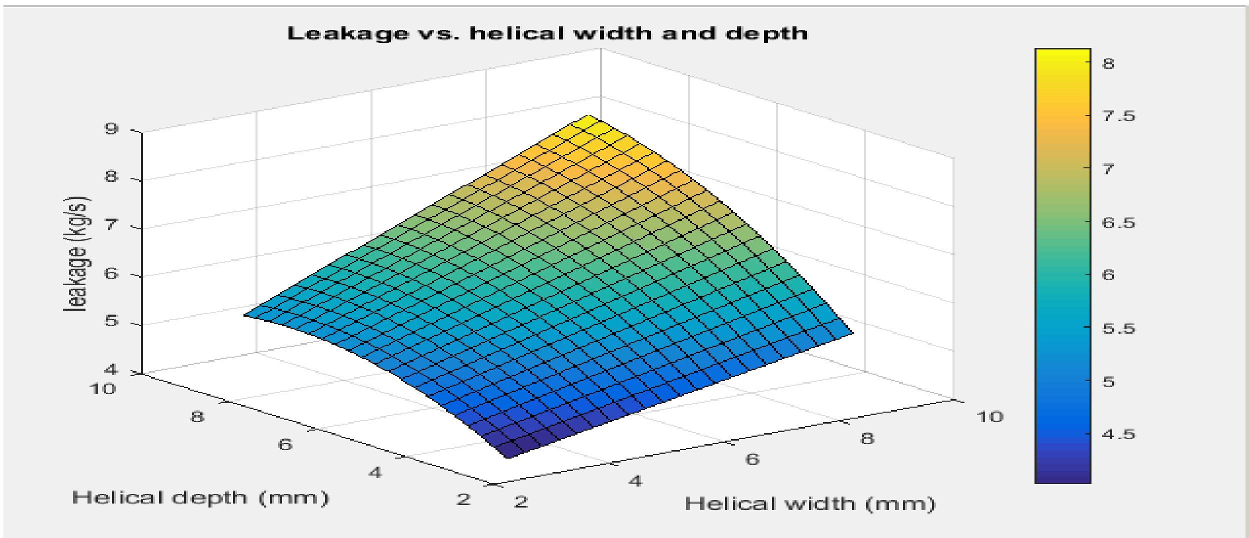

Figure 19: Leakage versus helical depth and width for helical groove stator and labyrinth rotor configuration

This is also the same relationship with groove size found in [11] for a seal with grooves on just one surface. Finally, Figure 20 and Figure 21 plot the leakage versus helix angle and number of labyrinth grooves for the helical groove rotor and labyrinth stator and helical groove stator and labyrinth rotor configurations, respectively.

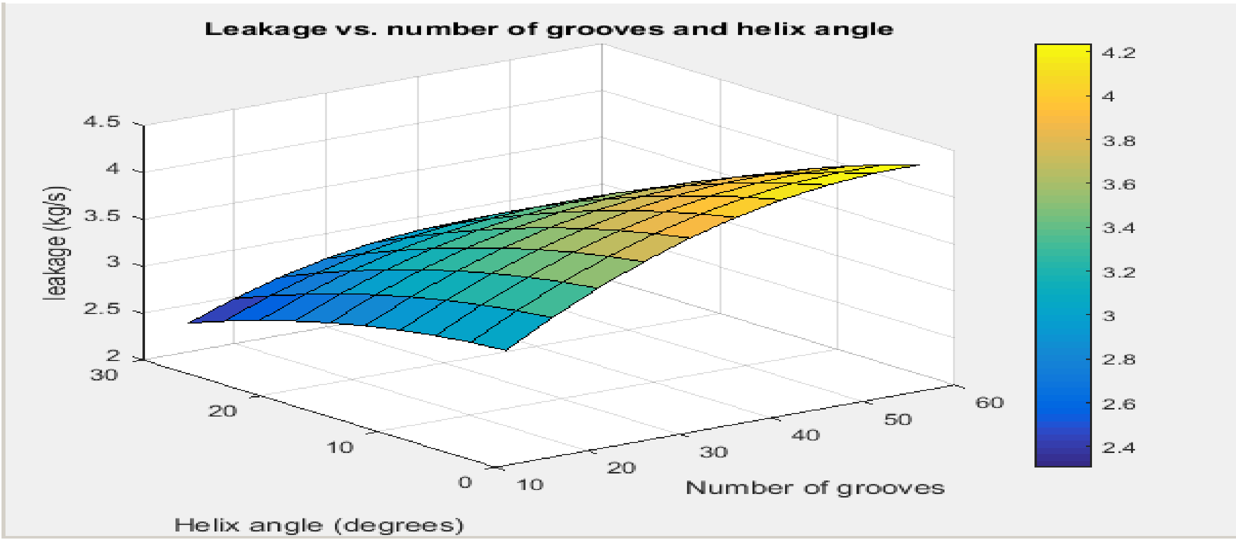

Figure 20: Leakage versus number of labyrinth grooves and helix angle for helical groove rotor and labyrinth stator configuration

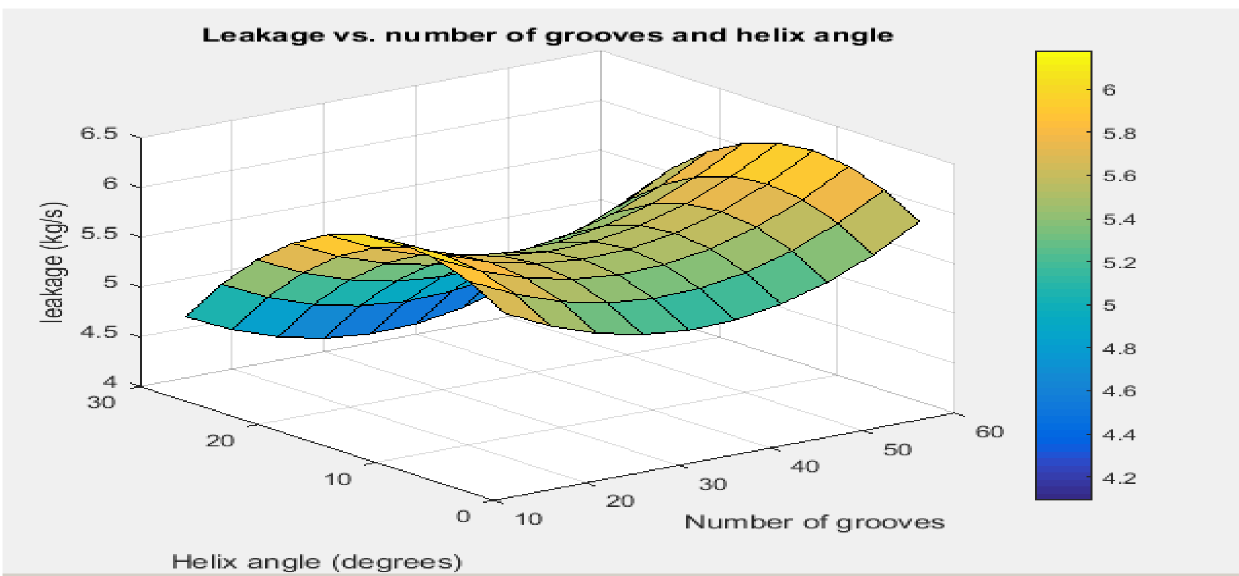

Figure 21: Leakage versus number of labyrinth grooves and helix angle for helical groove stator and labyrinth rotor configuration

The big difference in the influence of the number of grooves between the above two figures can be attributed to the fact that increasing the number of grooves increases the helix angle as given by equation 1. Since there is higher circular velocity in the seal with helical grooves on rotor, leakage is much lower in Figure 20 compared to Figure 21. Overall, the optimized design is shown in Figure 22.

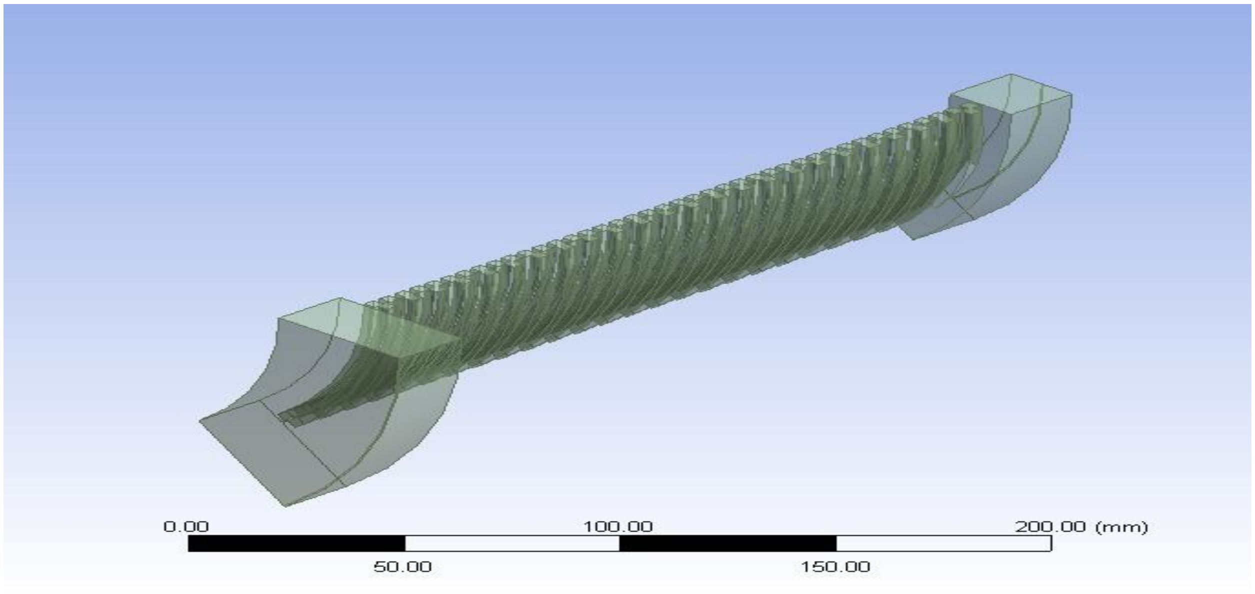

Figure 22: Optimized mixed helical groove and labyrinth seal

The leakage of the optimized seal design was estimated by the regression line as 13.36 kg/s and when that design was simulated, the actual leakage was 12.01 kg/s. That is an 11.2% difference which demonstrates the predictive power of the regression model. The leakage for an optimized helical groove seal with grooves on the stator is 19.05 kg/s as obtained from Watson et al in [11]. Thus, the mixed helical groove and labyrinth seal reduces the leakage by 45.3%. The hypothesis for the mechanism that reduces the leakage so substantially is that the interaction of the labyrinth grooves with the helical grooves contributes to the circumferential velocity in the seal, which leads to better pumping. The circumferential velocity is plotted for two designs in Figure 23.

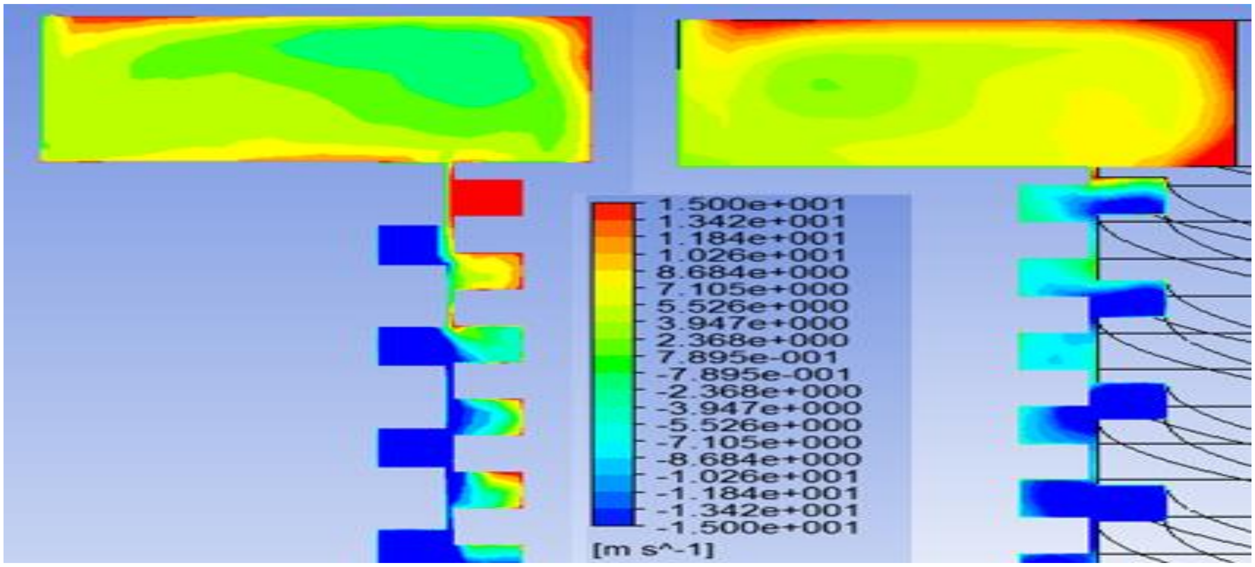

Figure 23: Circumferential velocity for mixed helical groove and labyrinth seals

On the right is a helical stator labyrinth rotor seal while the other design is shown on the left above. The circumferential velocity for the mixed designs above is substantially higher than the circumferential velocity on just the helical groove seals from [11] shown in Figure 24. The color plots were chosen based on maximum values rather than to match with each other so that a better comparison could be achieved based on those values.

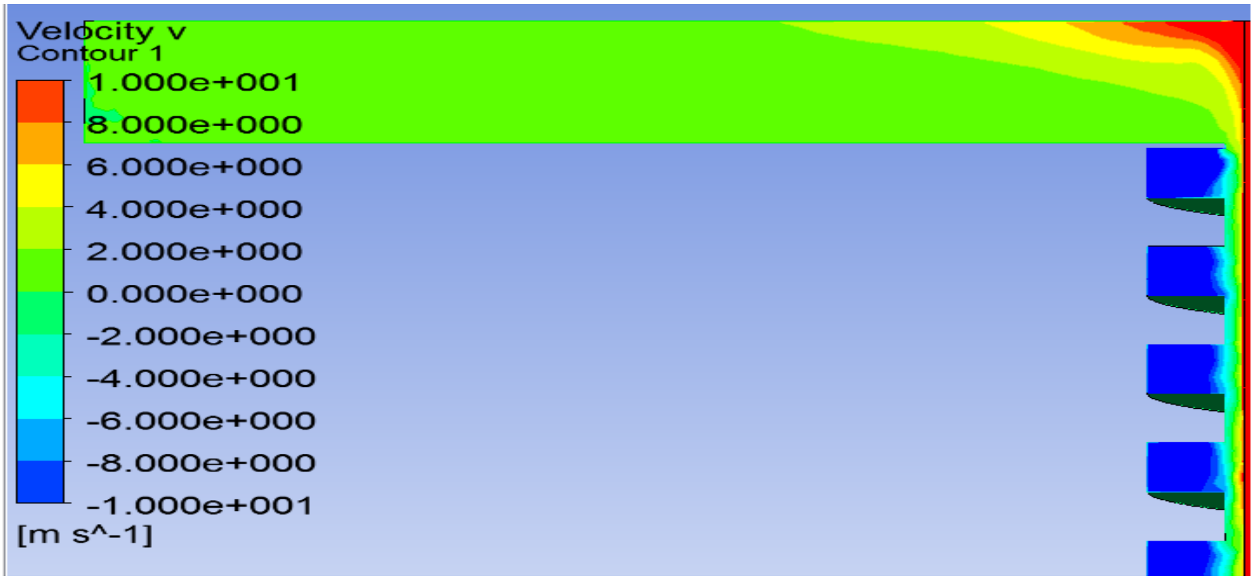

Figure 24: Circumferential velocity for helical groove seals with grooves on the stator [3]

CHAPTER 4: RESULTS – LOW PRESSURE CASE

The results presented in Chapter 3 showed that having grooves on both rotating and stationary surfaces of the seal significantly reduced leakage across the seal at high pressure. In this chapter, the analysis is done for a low pressure operating condition. Additionally, the reasons behind the results seen in the previous chapter are explained, and the study is extended to include the effect on power loss in the seal as well. To limit the number of designs required for the simulations, only the labyrinth surface parameters are varied in this study. The optimal helical surface design obtained in the previous study by Watson et al [7] was used for all the cases. The data obtained in this chapter was submitted to the Proceedings of the ASME 2018 International Mechanical Engineering Congress and Exposition (IMECE) and was accepted for presentation in November 2018 in Pittsburgh, PA.

Design of experiments

As mentioned, the design variables that were varied include labyrinth width (lw), labyrinth depth (ld), and number of labyrinth grooves (nlg). Helical groove depth and width and the helix angle were constant for all designs obtained from the optimal case found in [7].The range of values for these parameters is given in Table 9:

Labyrinth width (mm)	**Labyrinth depth (mm)**	**Number of labyrinth grooves**	**Helical width (mm)**	**Helical depth (mm)**	**Helix angle (degrees)**
1	1	25	2	2	3.8
2	2	50	2	2	3.8
3	3	70	2	2	3.8
4	4	90	2	2	3.8

Table 9: Range of values used for each design variable

There are 4^3 or 64 combinations of these design parameters for the proposed design. After removing the designs that violate the constraints given by equations (2) and (3), there remain a total of 44 designs to simulate. Out of those designs, 8 cases failed to reach convergence and were eliminated from the design space because there were sufficient remaining designs to perform the study. The baseline model has labyrinth depth and width of 4mm and 3mm respectively, 50 labyrinth grooves, and a helix angle of 4.7° for the constant helical stator surface.

DATA ANALYSIS

Based on the 36 successful simulations, two multifactor quadratic regression models were created and fitted into the leakage and power loss data. The three variables resulted in three quadratic terms, three linear terms, three cross terms, and a constant term. The original coefficients of the design variables for both leakage and power loss are shown in Table 10 and Table 11 respectively.

	Coefficients	*Standard Error*	*t Stat*	*P-value*
Intercept	-7.31E-03	9.24E-03	-7.90E-01	4.36E-01
nlg	-7.46E-04	1.37E-04	-5.45E+00	1.03E-05
nlg^2	3.31E-06	8.61E-07	3.84E+00	7.01E-04
lw^2	9.24E-04	6.49E-04	1.42E+00	1.66E-01
ld	-6.51E-03	3.38E-03	-1.93E+00	6.49E-02
ld^2	1.39E-03	4.46E-04	3.11E+00	4.49E-03
lw	3.87E-05	4.56E-03	8.49E-03	9.93E-01
ld*lw	-2.18E-03	5.74E-04	-3.79E+00	8.08E-04
ld*nlg	-3.95E-05	1.69E-05	-2.35E+00	2.69E-02
lw*nlg	7.15E-05	3.14E-05	2.28E+00	3.13E-02

Table 10: Initial coefficients of regression model for leakage data

	Coefficients	*Standard Error*	*t Stat*	*P-value*
Intercept	-1.41E+00	1.09E-01	-1.29E+01	8.48E-13
ld	1.55E-02	4.00E-02	3.87E-01	7.02E-01
ld^2	4.86E-03	5.27E-03	9.22E-01	3.65E-01
lw	6.86E-02	5.40E-02	1.27E+00	2.15E-01
lw^2	-1.62E-03	7.68E-03	-2.10E-01	8.35E-01
nlg	-1.74E-03	1.62E-03	-1.07E+00	2.93E-01
nlg^2	1.08E-05	1.02E-05	1.06E+00	2.99E-01
ld*lw	-2.61E-02	6.80E-03	-3.84E+00	7.10E-04
ld*nlg	-1.08E-03	1.99E-04	-5.41E+00	1.14E-05
lw*nlg	-6.23E-04	3.72E-04	-1.68E+00	1.06E-01

Table 11: Initial coefficients of regression model for power loss data

The regression analysis was performed using Microsoft Excel's© data analysis feature. This is different than in the high pressure case where the analysis was performed using Matlab© since there were significantly greater number of parameters, which MS Excel was unable to solve. As explained in Chapter 3, the t-statistic is obtained by taking the ratio of the coefficient to its error, which is then compared against a t-table to find the corresponding p-value. The p-values represent the probability of the term not being statistically significant. For this analysis, terms with p-values less than 0.05 are considered to have statistical significance. A backward regression process can be used to remove statistically insignificant variables from the model. In this regression process, the term with the highest p-value is discarded and a new model is calculated based on the remaining terms. This process is repeated until all of the variables have p-values of less than 0.05. The final coefficients for both leakage and power loss for the helical stator and labyrinth rotor model simulated in this study are presented in Table 12 and Table 13.

	Coefficients	*Standard Error*	*t Stat*	*P-value*
nlg	-7.46E-04	1.23E-04	-6.05E+00	1.86E-06
nlg^2	3.31E-06	8.42E-07	3.93E+00	5.31E-04
lw^2	9.29E-04	2.19E-04	4.23E+00	2.38E-04
ld	-6.52E-03	2.74E-03	-2.38E+00	2.45E-02
ld^2	1.39E-03	4.06E-04	3.41E+00	2.04E-03
ld*lw	-2.17E-03	4.41E-04	-4.93E+00	3.64E-05
ld*nlg	-3.95E-05	1.58E-05	-2.50E+00	1.90E-02
lw*nlg	7.17E-05	2.31E-05	3.10E+00	4.45E-03

Table 12: Final coefficients of regression model for leakage data

The R^2 value for the regression model for leakage data is 0.976. The final regression equation for leakage of the 1/13th sector model of the seal is:

$$\frac{\dot{m}}{13} = 0.0014 * ld^2 + 9.29 * 10^{-4} * lw^2 + 3.31 * 10^{-6} * nlg^2 - 0.00217(ld * lw) - 3.95 * 10^{-5}(ld * nlg) + 7.17 * 10^{-5}(lw * nlg) - 0.00652 * ld - 0.000746 * nlg \tag{7}$$

Similarly, the R^2 value for the regression model for power loss data is 0.969. The final model for power loss is:

	Coefficients	*Standard Error*	*t Stat*	*P-value*
Intercept	-1.43E+00	2.09E-02	-6.82E+01	1.84E-34
ld^2	7.27E-03	2.25E-03	3.22E+00	3.04E-03
lw	6.34E-02	1.19E-02	5.31E+00	9.74E-06
ld*lw	-2.38E-02	4.11E-03	-5.79E+00	2.51E-06
ld*nlg	-1.13E-03	1.10E-04	-1.03E+01	2.53E-11
lw*nlg	-8.20E-04	1.65E-04	-4.98E+00	2.43E-05

Table 13: Final coefficients of regression model for power loss data

$$\frac{P_{loss}}{13} = -0.007268 * ld^2 - 0.063366 * lw + 0.02381 * (ld * lw) + 0.00113 * (ld * nlg) + 0.00082 * (lw * nlg) + 1.4268 \tag{8}$$

DISCUSSION

Leakage

The regression equations above are used to create different response surfaces to analyze the impact of various labyrinth parameters on leakage and power loss. The plots of leakage versus labyrinth width and labyrinth depth at a specific number of grooves are presented in the figures below:

nlg: 25

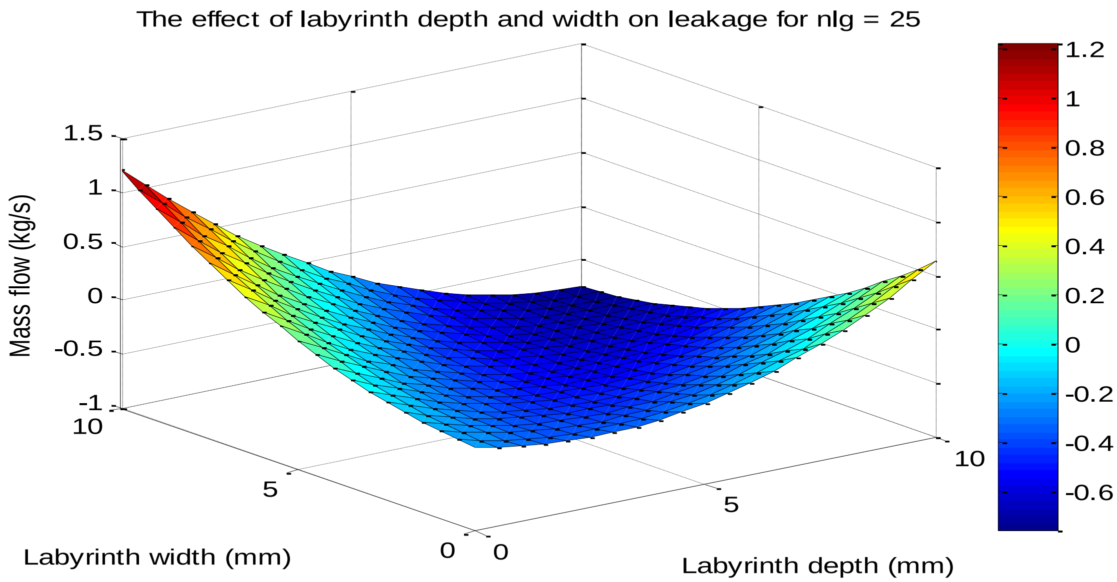

Figure 25: Leakage versus labyrinth depth and width with 25 grooves

nlg: 50

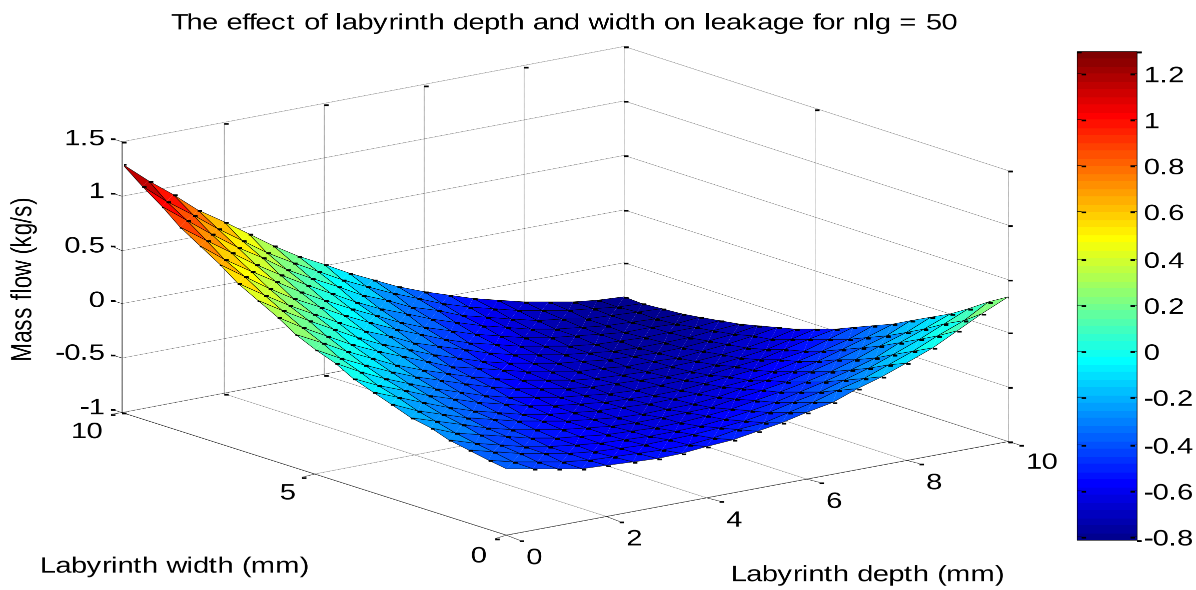

Figure 26: Leakage versus labyrinth depth and width with 50 grooves

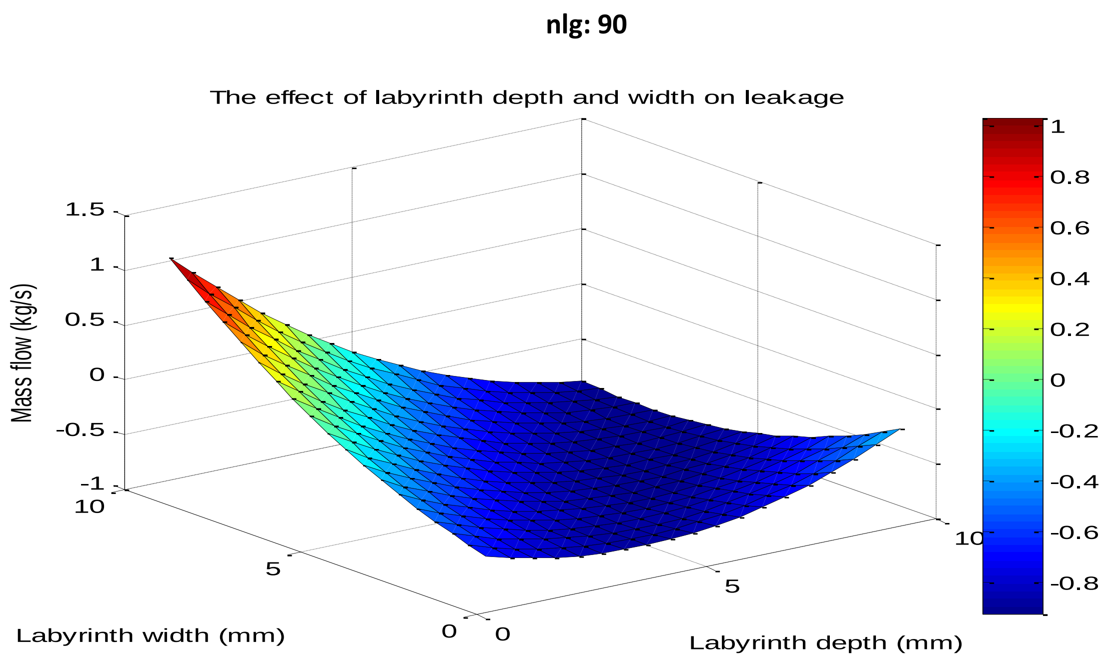

Figure 27: Leakage versus labyrinth depth and width with 90 grooves

Figures 25-27 show that leakage is significantly reduced by decreasing the labyrinth width which is consistent to what was discovered in [15]. The groove depth seems to have less of an impact on mass flow compared to width as can be seen from shallow slope with respect to depth. Furthermore, as the number of labyrinth grooves increases, it is important to note that the effect of groove depth and width diminishes but the overall leakage is decreased. This implies that having more grooves with smaller width and a medium depth of 5mm for the cases examined here is better in terms of leakage performance than having small number of wide grooves. To further analyze the impact of the number of grooves on mass flow, additional surface plots of leakage versus labyrinth width and number of grooves were plotted as shown in Figure 28 and Figure 29.

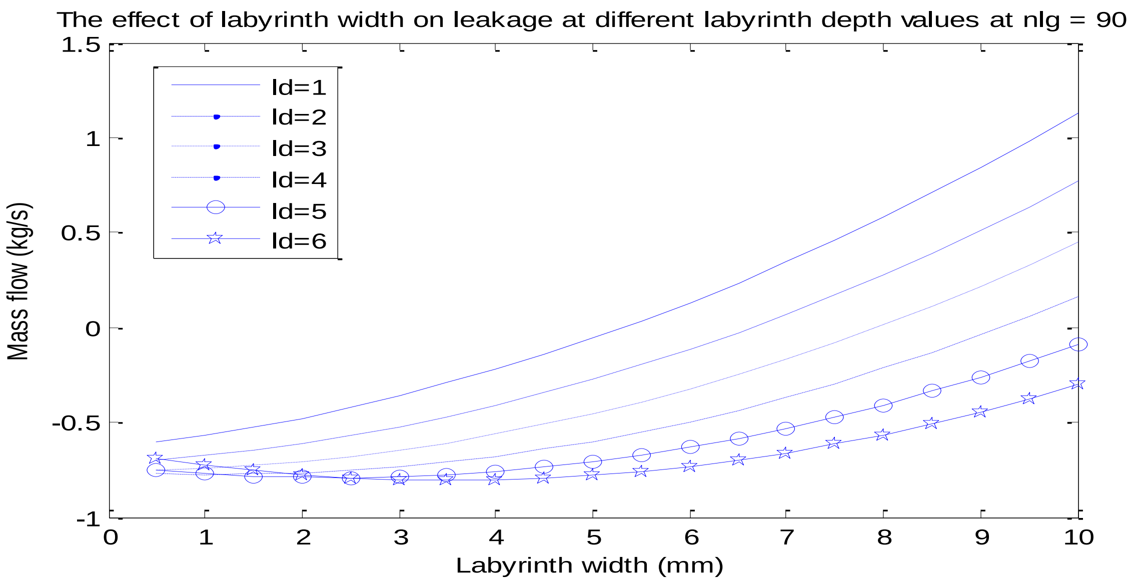

Figure 28: Leakage versus labyrinth width for 90 grooves and different labyrinth depth values

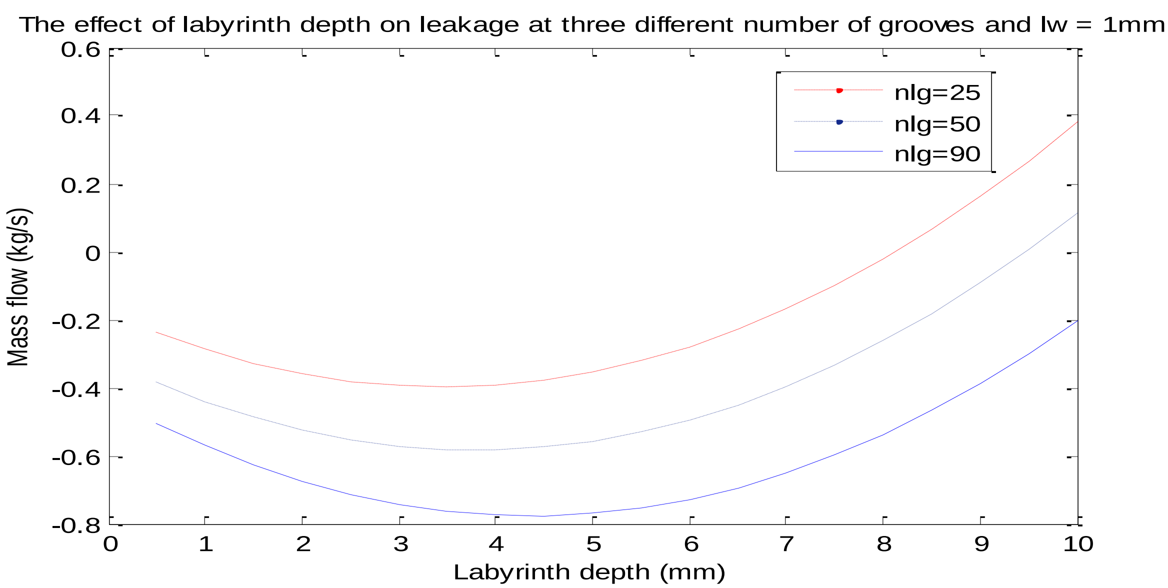

Figure 29: Leakage versus labyrinth depth for different number of grooves at lw = 1 mm

Thus, leakage is substantially reduced with increasing number of grooves and a decreased labyrinth width. Physically, this is an anticipated outcome since the fluid's interaction with many steeper grooves causes an increase in the dissipation of kinetic energy as it travels downstream, thus reducing leakage. On the contrary, there appears to be an optimal value of labyrinth depth as indicated by the inflection points on the plots above. Leakage decreases up until ld = 3 mm or ld

= 4 mm and quickly increases for depth values larger than 4 mm. This highlights the need to design the groove depth by first taking into account the other two groove parameters, and thus depends on the application being considered.

An important observation from the above figures that is worth noting is the negative leakage values in most of the designs. There are two possible theories in the literature that can explain the negative leakage obtained in this study. Firstly, this phenomenon was also recently explored in the bulk flow analysis performed in Watson et al [18], where it is explained purely as a numerical circumstance of the assumption that the fluid domain represents only a part of the seal length and leakage is actually approximately zero. This explanation is based on the experimental work by Anderson and Ludwig [1]. Secondly, a more plausible reason for such leakage values is because of a backflow that occurs in the jet stream region where the fluid is actually flowing upstream towards the inlet, especially for multistage pump applications. In order to allow that occurrence, both the inlet and outlet are treated as openings in this study.

Power loss

The power loss can be calculated from the shear stress of the rotor from the following relationship:

$$P_{loss} = U * \int_{0}^{L} \int_{0}^{2*pi} \tau(\theta, z) d\theta dz \quad . \qquad (9)$$

Here U is the fluid velocity and ɵ and z point to rotational and axial directions respectively.

Similar to leakage, the regression model developed in Equation 8 for power loss was used to create surface response plots in order to examine the effect of design variables on power consumption.

nlg: 25

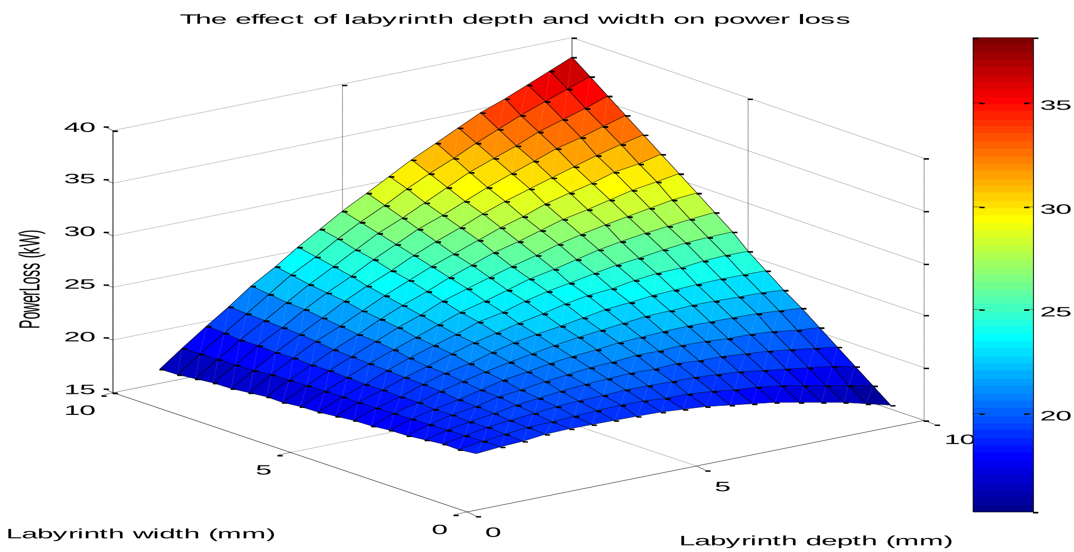

Figure 30: Power loss versus labyrinth depth and width with 25 grooves

nlg: 90

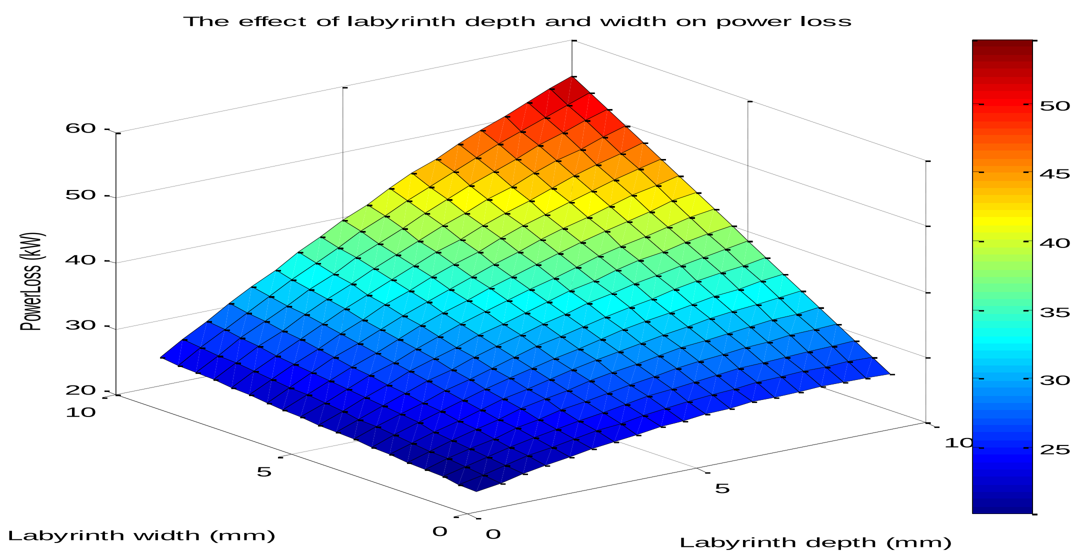

Figure 31: Power loss versus labyrinth depth and width with 90 grooves

It can be observed from Figure 30 and Figure 31 that power loss increases significantly with an increase in the number of grooves as well as the groove width. This is the anticipated outcome since more grooves as well as wider grooves lead to an increase in energy losses and thus an increase in power consumption. This relationship can be better observed in the plots of power loss versus labyrinth depth at different values of labyrinth width as displayed in Figure 32.

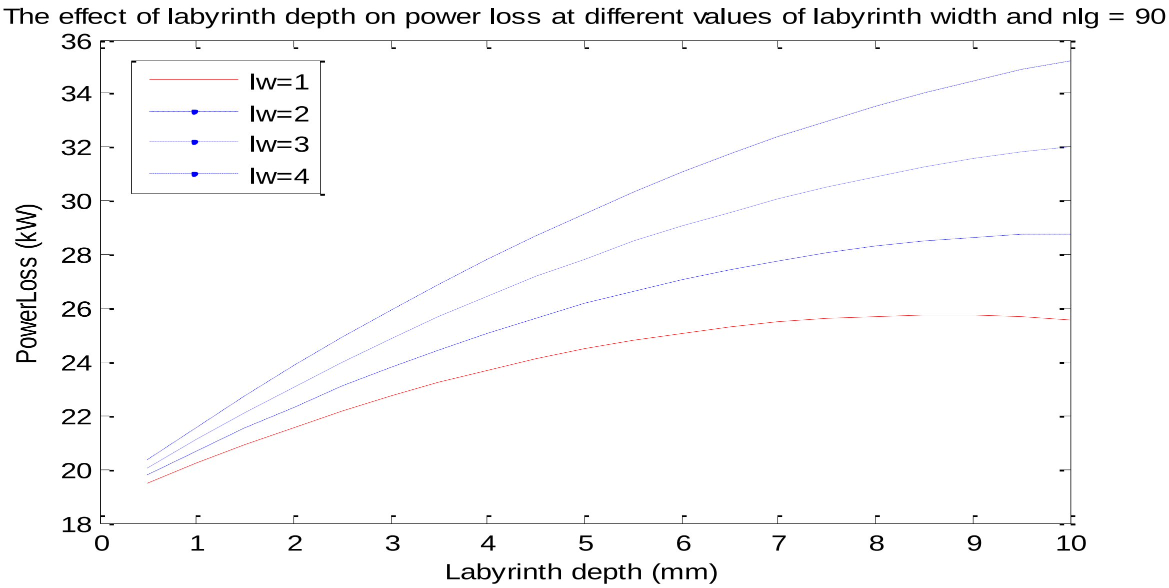

Figure 32: Power loss versus labyrinth depth at different values of labyrinth width

The minimum power loss occurs at smallest value of labyrinth depth as well as labyrinth width. Next, power loss is plotted against labyrinth depth at the optimal width value of 1 mm in Figure 33. Power loss decreases with an increase in labyrinth depth for fewer numbers of grooves. However, since leakage increases significantly for seals with fewer grooves as seen above, the optimal labyrinth depth for power loss must be determined at large number of grooves.

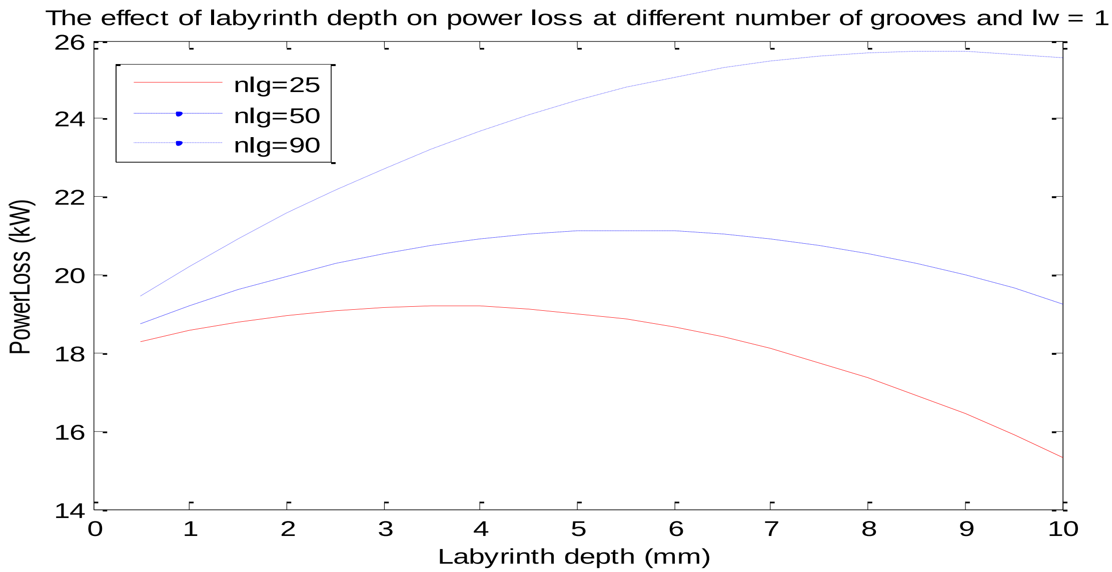

Figure 33: Power loss vs. labyrinth depth at different number of grooves

The effect of groove depth on power loss can be explained well with the streamlines of the flow as shown in Figure 34 and Figure 35.

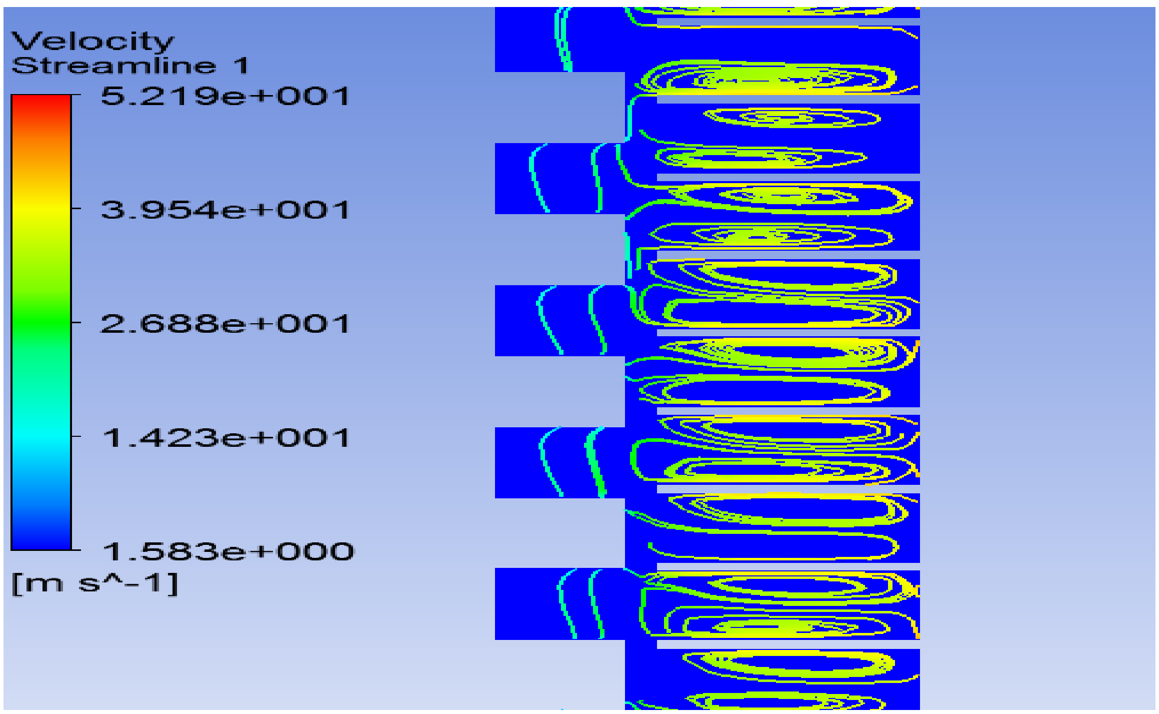

Figure 34: Flow streamlines for the design with big labyrinth groove depth

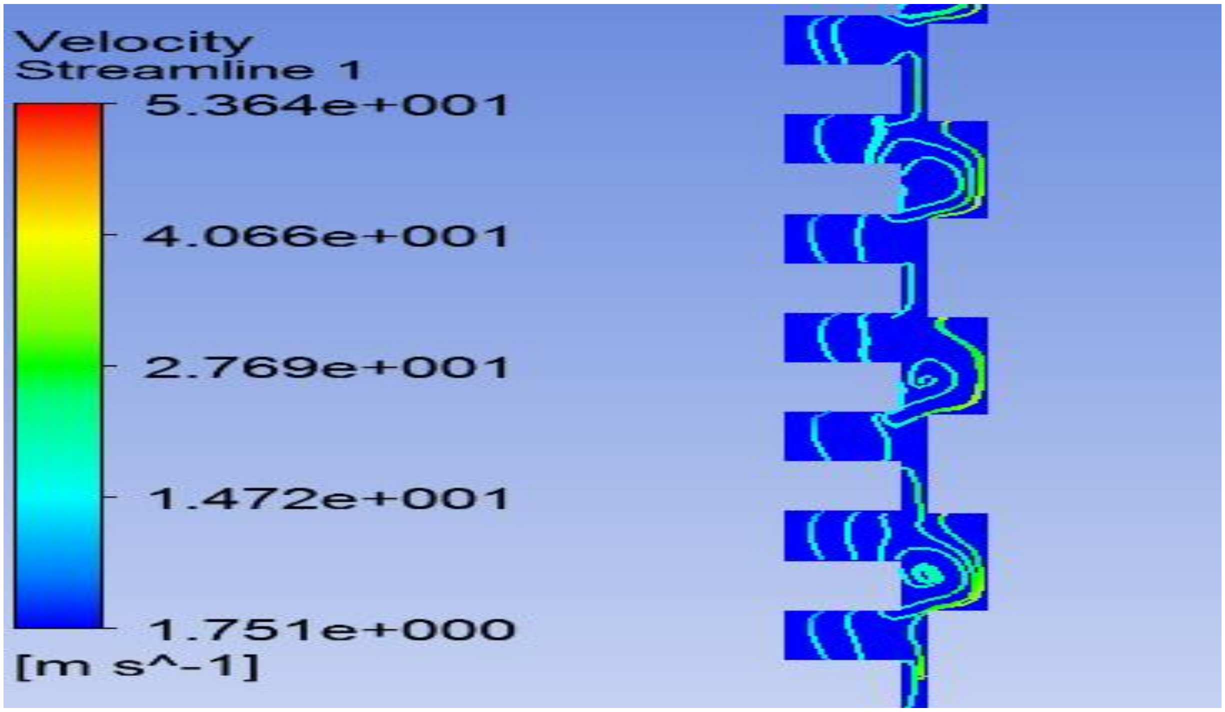

Figure 35: Flow streamlines for the design with small labyrinth groove depth

For taller labyrinth grooves, the vorticies are well contained within the grooves and have little to no influence in the jet stream region as seen on Figure 34. The vorticies inside the grooves lead to an increase in shear stress which then causes an increase in power as explained by Equation 6. However, for shorter grooves, the vorticies travel well into the jet stream region causing very little shear stress on the rotor which leads to lower power loss.

Optimal Design

The optimal design was determined by calculating the efficiency of the seal obtained from the ratio of mass flow and power loss. The plot of leakage versus power loss is shown in Figure 36.

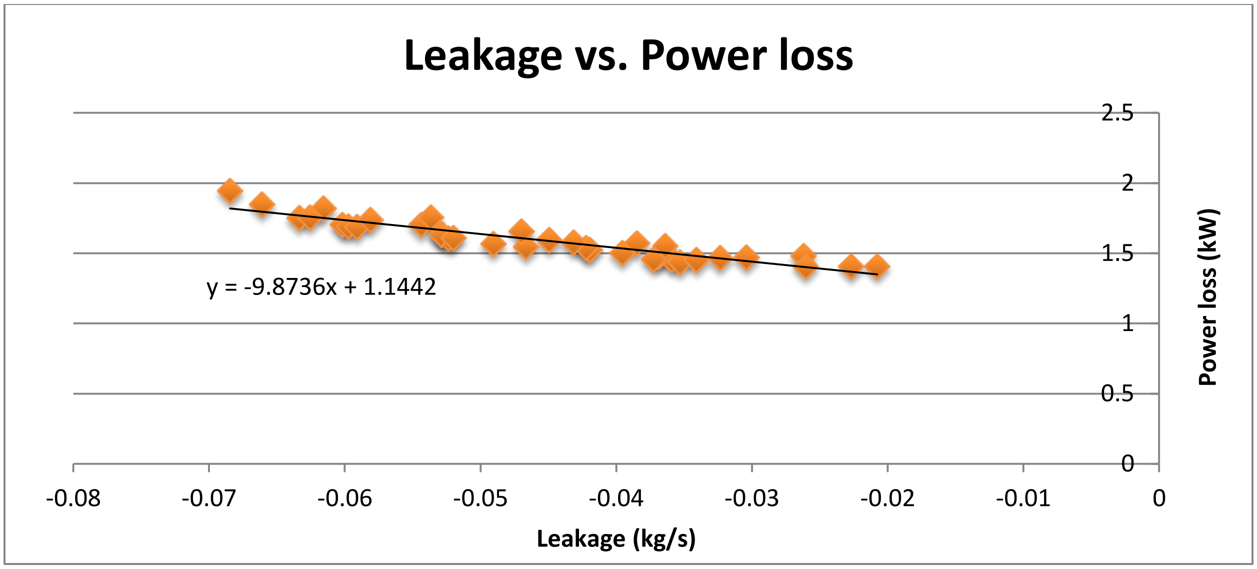

Figure 36: Leakage versus power loss

Both leakage and power loss were first non-dimensionalized by dividing each of the values by the leakage and power loss of the optimized helical stator seal. Next, the efficiency was calculated by dividing the non-dimensional leakage by the non-dimensional power loss. Based on the highest efficieny calculated, the optimal design was determined to be the one with a labyrinth depth of 3 mm, labyrinth width of 1 mm, and 90 labyrinth grooves. The leakage value obtained for the optimized seal is -0.823 kg/s which is 194% lower than the value obtained for the optimized helical seal in [7] with a leakage of -0.012 kg/s. The power loss for the optimized labyrinth rotor helical stator seal is 22.78 kW which is 26.2% higher than the optimized helical only value of 17.5 kW. Even though adding a labyrinth rotor causes a slight increase in power loss, the overwhelming improvement in leakage leads to an increase in the overall efficiency of the machine. The sector model of the optimized design is shown in Figure 37.

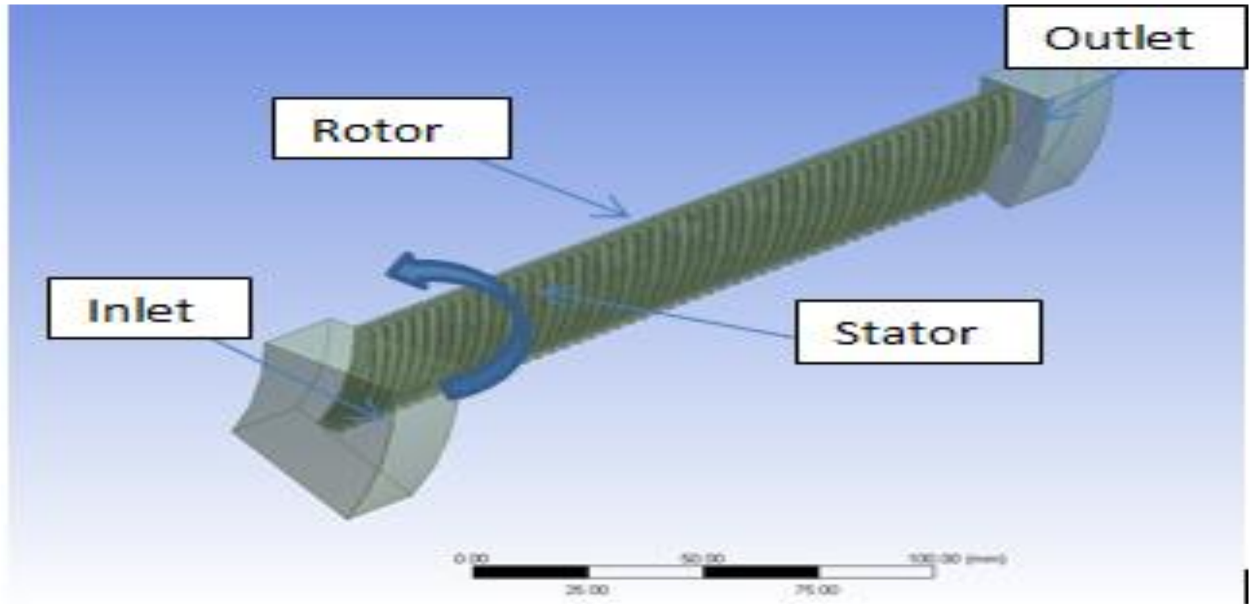

Figure 37: Optimized labyrinth rotor helical stator seal

The source of leakage reduction for the mixed labyrinth rotor helical stator seal can be examined through the circumferential velocity and the axial pressure distribution. The circumferential velocity is correlated to the pumping effect of the helical grooves and has been shown to increase by having labyrinth grooves on the rotor. Figure 38 and Figure 39 show the circumferential velocity at the rotor stator interface for optimized helical only and optimized labyrinth rotor helical stator designs.

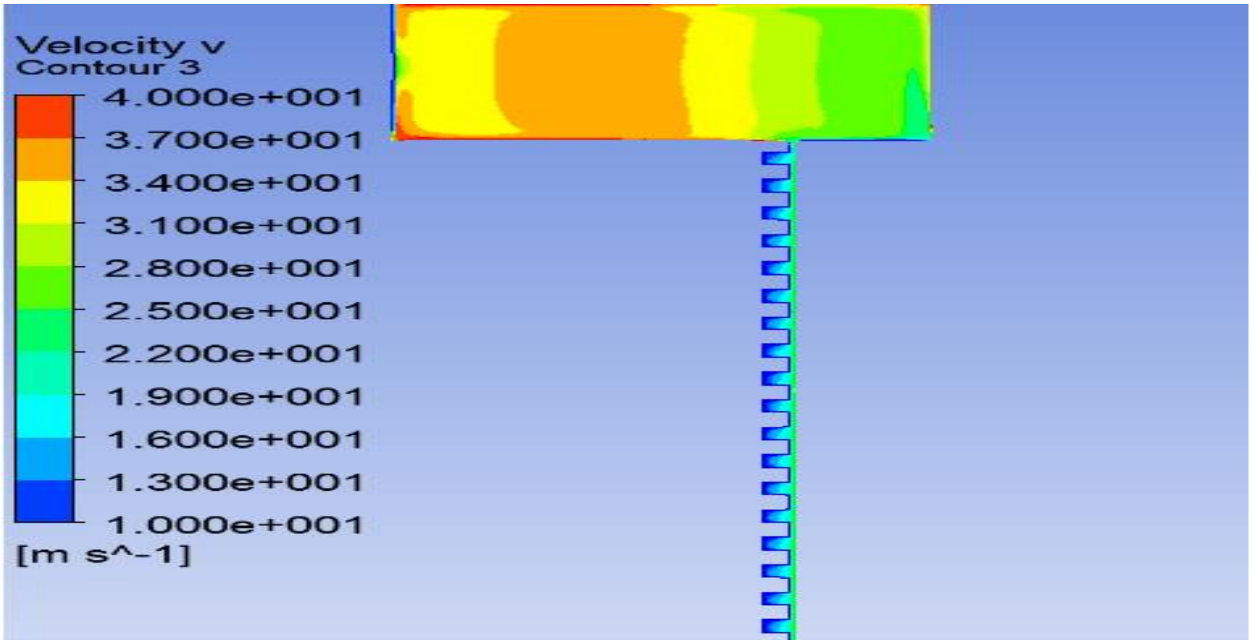

Figure 38: Circumferential velocity of optimized helical seal

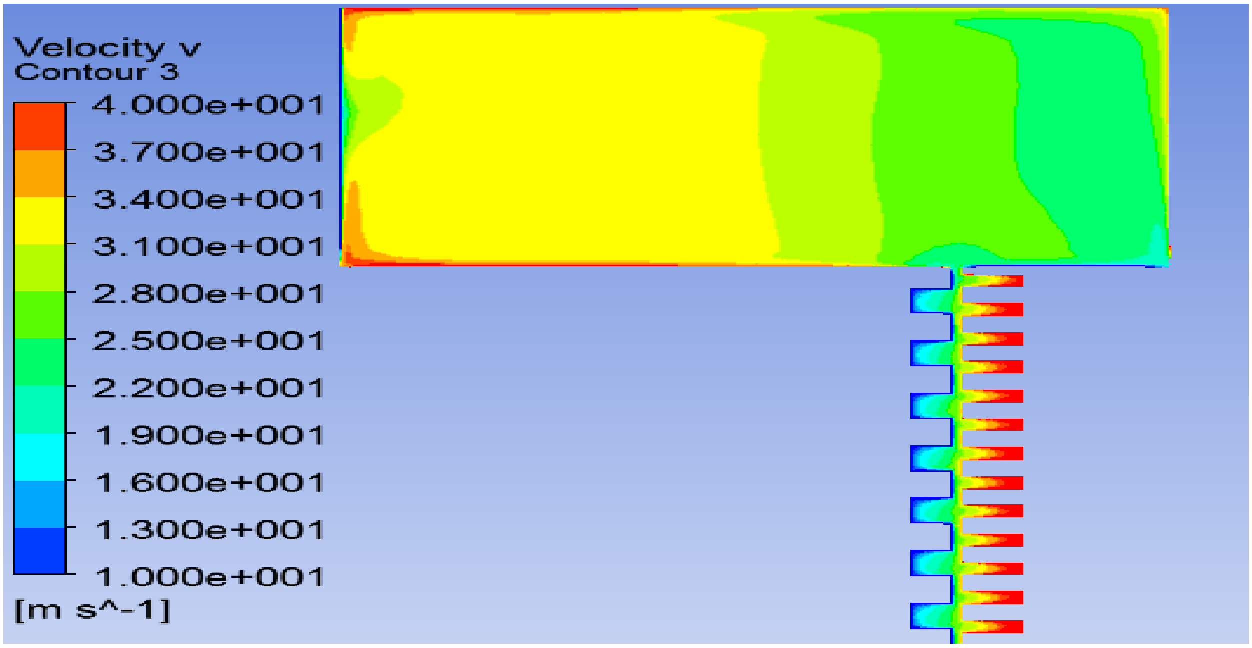

Figure 39: Circumferential velocity of optimized labyrinth rotor helical stator seal

The average circumferential velocity of the mixed case is 30.06 m/s while the average for the helical only case in Figure 38 is 19.67 m/s. The labyrinth rotor surface in Figure 39 has a constant circumferential velocity, which clearly increases the pumping action of the helical grooves as affirmed by the higher velocity value.

Additionally, adding a labyrinth surface increases the expansion and contraction of fluid as it flows downstream of the seal which leads to a rise in kinetic energy dissipation and thus lower leakage flow. The axial pressure profile of the optimal helical only case is presented in Figure 40.

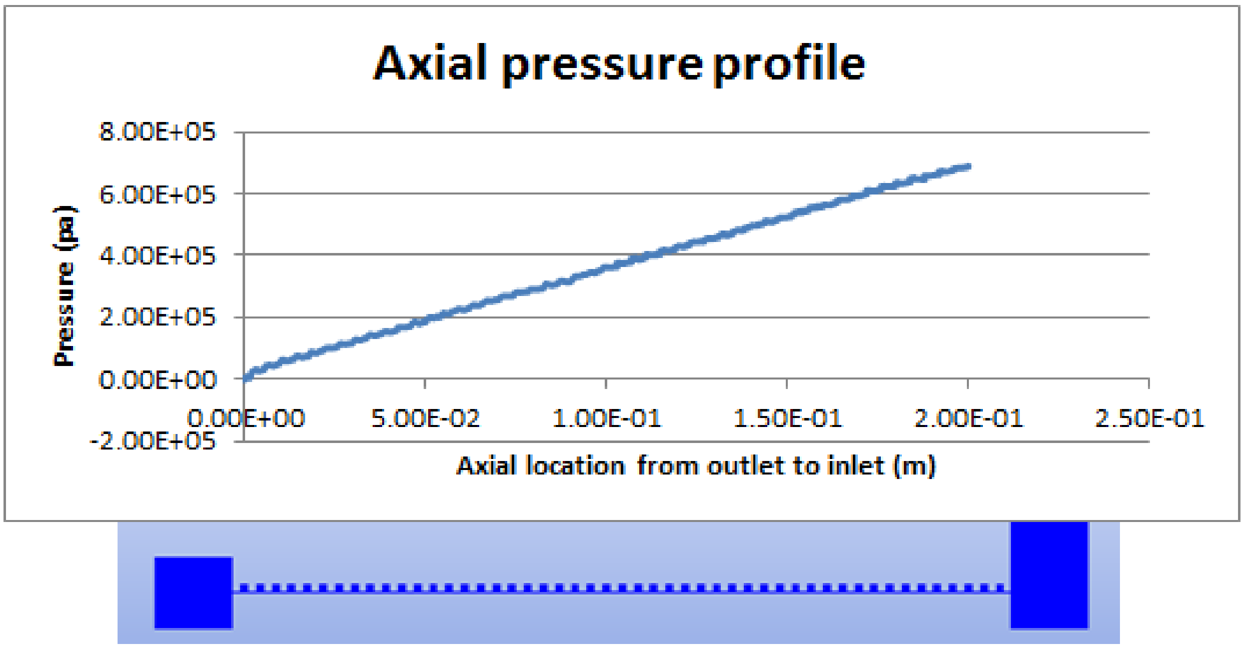

Figure 40: Axial pressure profile for optimized helical only design

The plot shows the decrease in pressure from inlet to outlet with fluctuations in the values indicated by mini spikes at each of the groove locations. This disturbance in pressure is where the fluid is expanding and contracting due to the grooves. Therefore, adding a labyrinth surface and thus additional grooves along the fluid path would cause further disturbances in the pressure axially along the seal, resulting in lower leakage rates.

CHAPTER 5: CONCLUSIONS AND FUTURE WORK

Summary and Conclusions

Overall, this study demonstrates that mixed helical groove and labyrinth seal designs have the potential to dramatically reduce leakage across a pressure differential and therefore improve the efficiency of the machines. In Chapter One, the physical and geometric features of the mixed seals are discussed and the primary objective of the study is defined. Previous studies in literature suggest that having grooves in both the rotor and stator surfaces of the seal significantly reduce the amount of leakage compared to seals that have grooves on just one surface. In this work, the author investigated the impact of having different types of grooves on the rotor and stator surfaces in terms of leakage as well as power loss reduction of the seal. Chapter Two presents the approach taken to perform the analysis and reach the desired understanding. Two different pressure cases are considered and the results of the high pressure case are presented in Chapter Three while the results of the low pressure case are presented in Chapter Four. At high pressure, the optimized helical rotor and labyrinth stator design had 45.3% less leakage than an optimized helical groove seal with grooves just on the stator. The range of leakage values were 57.58 kg/s to 12.01 kg/s which agrees with the literature that optimization of seal design is particularly important for helical groove seals [11]. Furthermore, this thesis illustrates that adding a labyrinth surface to an optimal helical seal can substantially reduce leakage across both a high and as well as low pressure differential. This decrease in leakage can be attributed to the streamlines and circumferential velocity of the flow. The power loss is increased by approximately 26 % for the mixed seal design; however, the huge improvement in leakage leads to an increase in overall efficiency of the machine. The most important parameter for such improvement in leakage is deemed to be the number of labyrinth grooves on the rotor which highlights the importance of including the number of grooves in seal optimization studies.

Some of the key discoveries made from this work are as follows. Due to a significant reduction in leakage observed for these mixed helical-labyrinth seals, they would be exceptional replacements to the current sealing technology used at high pressure applications such as in centrifugal pumps. Whether these pumps are used in buildings for pumping general water supply, sewage, or in fire protection systems and chemical industries, leakage can be kept at a minimum by applying the mixed grooved seals. Furthermore, since zero leakage of fluid is observed at low pressure, these seals could also be implemented in a machine as end seals, where fluid leakage would otherwise drastically reduce the lifespan of bearings that are normally used at the ends. Likewise, the zero leakage capability of these seals makes them suitable candidates for sealing supercritical CO_2 applications. Thus, the mixed helical-labyrinth seals have the potential to not only change the future of pumping industry but could also indirectly play a huge role in making the environment cleaner. The fact that the rotor and stator surfaces can be optimized separately as demonstrated in this study makes them even more adaptive to the desired application.

Future Work

Future work will need to evaluate the rotor dynamic performance of mixed helical groove and labyrinth seal designs. The work by Kim and Childs suggests that helical groove seals with grooves on one surface are generally more stable than other types of seals, so adding a labyrinth surface may negatively impact the stability of the seal [3]. This is especially a concern given the higher circumferential velocities found here. In order to quantify the threat that the mixed seals possess in terms of machine stability and comprehend the severity of the increase in circumferential velocities, an initial theoretical assessment is conducted based on previous findings by Iwatsubo et al [5]. In this study, the authors experimentally determine the static and dynamic characteristics of helical groove seals. The effect of circumferential velocity on radial and tangential forces of the seals is plotted as shown below in Figure 41.

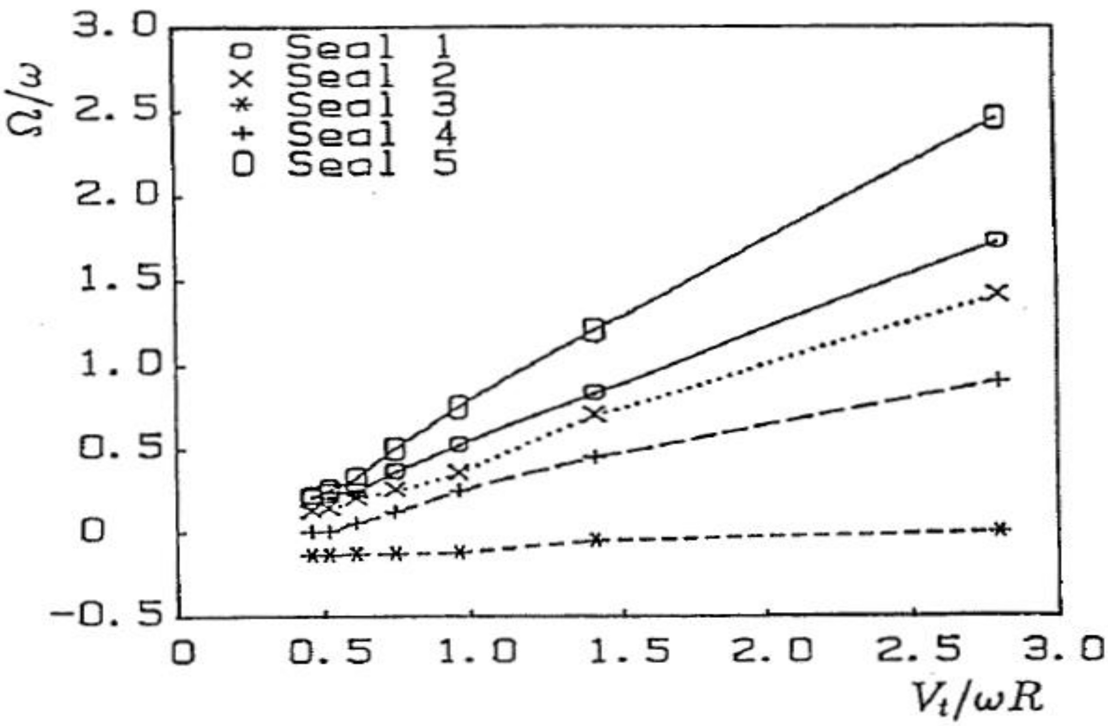

Figure 41: Upper limit of unstable area for positive pre-swirl velocity [5]

In the figure above, seal 3 has helical stator, smooth rotor with a helix angle of 3.32 degrees, which is the closest to the seal model developed in this study. The plot shows the upper limits of unstable area, or the approximated intersections between the destabilizing force, F_θ, and axis of Ω/ω, the ratio of circumferential velocity and rotor speed, for different positive pre-swirl velocities. Seal 3 has the minimum of the upper limit indicating that it has the best effect on rotor stability. However, for all the seal types considered, as long as the circumferential velocity is less than three times the rotor speed, the machine will remain stable for forward whirl modes. This is clearly the case for the mixed seals studied in this thesis. The rotor speed of 5000 rpm with a 0.1 m radius or 52 m/s is well below 3 times the highest circumferential velocity of 30 m/s that was observed in Chapter 4. Thus, while the mixed seals lead to an increase in destabilizing forces, they will not significantly harm the operation of the machine as long as they are designed within the scope of the operating conditions. Nonetheless, a complete rotor-dynamic analysis of these seals will need to be completed in the future for a thorough understanding of their behavior.

Additionally, the findings of this study for the mixed seal case will need to be validated experimentally in the future. The seals test rig that is under development at the ROMAC lab will be used to conduct the experimental work on these seals. The test rig is designed with a replaceable test section which allows testing of multiple seal types and designs. Currently, only smooth and various seal patterns on the stator section can be tested. However, it can easily be modified to conduct tests with seal patterns on the rotor or mixed seal designs that form the core of this work. The leakage, power loss, temperature, and pressure change data can all be obtained from the test rig and compared against the CFD data presented in this thesis to ensure the accuracy of the results obtained. In order to ensure the stability of the rig, preliminary cases have been modelled using in-house ROMAC software, Damper Seal and Rotstb. Once the final assembly and modeling of the rig is complete, the data that will be gathered using various seal designs will undoubtedly be a significant addition to literature.

NOMENCLATURE

α –Helix angle for grooves	[degrees]
w –Groove width	[mm]
d –Groove depth	[mm]
ha –Helix angle	[degrees]
lw –Labyrinth groove width	[mm]
ld –Labyrinth groove depth	[mm]
hw – Helical groove width	[mm]
hd–Helical groove depth	[mm]
nlg–Number of labyrinth grooves	[no unit]
R_{rotor}–Rotor radius	[mm]
R_{stator}–Stator radius	[mm]
N –Number of grooves	[no unit]
s –Spacing	[mm]
Ω –Rotor speed	[rpm]
P_i –Inlet pressure	[MPa]
P_o–Outlet pressure	[MPa]
$\dot{m}$–leakage	[kg/s]
L –Seal length	[mm]
τ – Shear stress	[Pa]
U – Fluid velocity	[m/s]

REFERENCES

[1] W. J. Anderson and L. P. Ludwig, "Bearing and Seal Technology," NASA Lewis Research Center, Cleveland, OH, 1968.

[2] D. W. Childs, "SSME Seal Test Program: Leakage Tests for Helically-Grooved Seals," NASA Center for Aerospace Information (CASI), 1983.

[3] C. H. Kim and D. W. Childs, "Analysis for Rotordynamic Coefficients of Helically-Grooved Turbulent Annular Seals," *Journal of Tribology,* no. 109(1), pp. 136-143, 1987.

[4] D. W. Childs, S. A. Nolan and J. J. Kilgore, "Test Results for Turbulent Annular Seals, Using Smooth Rotors and Helically Grooved Stators," *Journal of Tribology,* vol. 112, pp. 254-258, 1990.

[5] T. Iwatsubo, B. C. Sheng and M. Ono, "Experiment of Static and Dynamic Characteristics of Sprial Grooved Seals," in *NASA. Lewis Research Center, Rotordynamic Instability Problems in High-Performance Turbomachinery*, 1991.

[6] C. Watson and H. G. Wood, "Optimizing a Helical Groove Seal with Grooves on Both the Rotor and Stator Surfaces," in *ASME Turbo Expo 2017: Turbomachinery Technical Conference and Exposition*, Charlotte, NC, 2017.

[7] C. Watson and H. Wood, "Developing an Optimal Helix Angle as a Function of Pressure for Helical Groove Seals," in *Proceedings of the 9th International Symposium on Pumping Machinery*, Waikoloa, Hawaii, USA, 2017.

[8] C. Watson and H. Wood, "Experimental Validation of Computational Fluid Dynamics (CFD) for Modeling Leakage Performance of Helical Groove Seals," *Journal of Tribology.*

[9] M. Zhang, X.-f. Wang, S.-l. Xu and S. Yin, "Leakage Characteristic of Helical Groove Seal Design in Reactor Coolant Pump," *International Journal of Rotating Machinery,* vol. 2012, no. 619459, p. 8, 2012.

[10] S. P. Asok, K. Sankaranarayanasamy, T. Sundararajan, G. Vaidyanathan and K. K. Udhaya , "Pressure Drop and Cavitation Investigations on Static Helical-Grooved Square, Triangular and Curved Cavity Liquid Labyrinth Seals," *Nuclear Engineering and Design,* pp. 843-853, 2011.

[11] C. Watson and H. Wood, "Optimizing a Helical Groove Seal Using Computational Fluid Dynamics," in *Proceedings of EDF-Pprime*, Futuroscope Chasseneuil, France, 2016.

[12] V. G. Kaya, V. Temiz, Z. Parlar and L. Kavurmacioglu, "Design of a New Non-Contact Screw Seal and Determination of Performance Characteristics," in *Proceedings of the World Congress on Momentum, Heat and Mass Transfer (MHMT '16)*, Istanbul, Turkey, 2016.

[13] T. Cebeci and A. M. Smith, Analysis of Turbulent Boundary Layers, New York: Academic Press, Inc., 1974.

[14] M. Ariff, S. Salim and C. S. Cheah, "Wall Y+ Approach for Dealing with Turbulent Flow Over a Surface Mounted Cube: Part1- Low Reynolds Number"," in *Seventh International Conference on CFD in the Minerals and Process Industries*, 2009.

[15] W. Paudel, C. Watson and H. Wood, "Mixed Helical Labyrinth Groove Seal Optimization Using Computational Fluid Dynamics," in *Proceedings of ASME Turbo Expo 2017: Turbomachinery Conference and Exposition*, Charlotte, NC, USA, 2017.

[16] R. W. Kennard and L. A. Stone, "Computer Aided Design of Experiments," *Technometrics,* no. 11(1), pp. 137-148, 1969.

[17] M. A. Efroymson, "Multiple Regression Analysis, Mathematical Methods for Digital Computers," Ralston A. and Wilf, H.S., (eds), Wiley, NY, 1960.

[18] C. Watson, A. Untaroiu, N. Morgan, H. Jin, B. Weaver and H. Wood, "Response Surface Mapping of Performance for Helical Groove Seals with Incompressible Flow," in *Proceedings of ASME Turbo Expo 2016: Turbine Technical Conference and Exposition*, Seoul, South Korea, 2016.

[19] D. W. Childs, S. A. Nolan and J. J. Kilgore, "Test Results for Turbulent Annular Seals, Using Smooth Rotors and Helically Grooved Stators," *ASME Journal of Tribology (89-Trib-11),* 1989.

[20] Z. Li, J. Li and Z. Feng, "Numerical Investigation on the Leakage and Static Stability Characteristics of Pocket Damper Seals at High Eccentricity Ratios," in *Proceedings of ASME Turbo Expo 2017: Turbomachinery Conference and Exposition*, Charlotte, NC, USA, 2017.

[21] C. Watson, W. Paudel, B. Weaver and H. Wood, "Quantifying the Linearity of the Fluid Dynamics for Non-Contacting Annular Seals," in *Proceedings of ASME IMECE 2016: International Mechanical Engineering Congress and Exposition*, Phoenix, AZ, USA, 2016.

[22] M. J. Daigle, A. Bregon and I. Roychoudhury, "Distributed Prognostics Based on Structural Model Decomposition," *IEEE Transactions on Reliability,* vol. 63, no. 2, pp. 495-510, 2014.